nature communications

Article

https://doi.org/10.1038/s41467-024-53844-8

Preoperative methionine restriction induces perivascular adipose tissue browning and improves vein graft remodeling in male mice

Received: 7 December 2023

Accepted: 24 October 2024

Published online: 07 November 2024

Check for updates

Peter Kip[1,2,3,4,11], Thijs J. Sluiter[1,2,3,4,11], Michael R. MacArthur[2,5], Ming Tao[1], Nicky Kruit[3,4,6], Sarah J. Mitchell[7], Jonathan Jung[2,8], Sander Kooijman[6], Josh Gorham[9], Jonathan G. Seidman[9], Paul H. A. Quax[3,4], Julius L. Decano[10], Masanori Aikawa[10], C. Keith Ozaki[1], James R. Mitchell[2] & Margreet R. de Vries[1,3,4]

Short-term preoperative methionine restriction (MetR) is a promising translatable strategy to mitigate surgical injury response. However, its application to improve post-interventional vascular remodeling remains underexplored. Here we find that MetR protects from arterial intimal hyperplasia in a focal stenosis model and pathologic vascular remodeling following vein graft surgery in male mice. RNA sequencing reveals that MetR enhances browning in arterial (thoracic aorta) perivascular adipose tissue (PVAT) and induces it in venous (caval vein) PVAT. Specifically, *Ppara* is highly upregulated in PVAT-adipocytes upon MetR. Furthermore, MetR dampens the postoperative pro-inflammatory response to surgery in PVAT-macrophages in vivo and in vitro. This study shows that the detrimental effects of dysfunctional PVAT on vascular remodeling can be reversed by MetR, and identifies pathways involved in MetR-induced browning of PVAT. Furthermore, we demonstrate the potential of short-term preoperative MetR as a simple intervention to ameliorate vascular remodeling after vascular surgery.

Revascularization surgery remains a mainstay in the treatment of arterial occlusive disease[1], however, these interventions are hampered by high failure rates which frequently originate from intimal hyperplasia (IH) and adverse vascular remodeling[2]. This pathophysiological response to surgical injury is defined by initial endothelial dysfunction and leukocyte transmigration[2,3] followed by vascular smooth muscle cell (VSMC) migration and proliferation, ultimately occluding the artery or vein graft[2,4]. Despite decades of research, therapies to abrogate adverse vascular remodeling responses following an intervention remain limited.

Perivascular adipose tissue (PVAT) surrounding blood vessels functions as a paracrine organ with the potential for impacting post-interventional vascular remodeling[5,6]. Interestingly, preclinical work suggests inflamed PVAT driven by obesity can accelerate IH[6]. For example, high-fat diet (HFD) in mice increases the secretion of interleukin (IL)-6, IL-8 and C-C motif ligand 2 (CCL2) from perivascular

[1]Department of Surgery, Brigham & Women's Hospital, Harvard Medical School, Boston, MA, USA. [2]Department of Molecular Metabolism, Harvard T.H. Chan School of Public Health, Boston, MA, USA. [3]Einthoven Laboratory for Experimental Vascular Medicine and Regenerative Medicine, Leiden University Medical Center, Leiden, The Netherlands. [4]Department of Surgery, Leiden University Medical Center, Leiden, The Netherlands. [5]Lewis-Sigler Institute for Integrative Genomics, Princeton University, Princeton, NJ, USA. [6]Division of Endocrinology, Department of Medicine, Leiden University Medical Center, Leiden, The Netherlands. [7]Ludwig Princeton Branch, Ludwig Institute for Cancer Research, Princeton University, Princeton, NJ, USA. [8]Department of Surgery, University of Pennsylvania, Philadelphia, PA, USA. [9]Department of Genetics, Harvard Medical School, Boston, MA, USA. [10]Center for Interdisciplinary Cardiovascular Sciences, Cardiovascular Division, Department of Medicine, Harvard Medical School, Boston, MA, USA. [11]These authors contributed equally: Peter Kip, Thijs J. Sluiter. e-mail: M.R.de_Vries@lumc.nl

adipocytes[7]. After carotid wire injury, cohorts with inflamed adipose tissue induced by HFD had exacerbated IH[8,9].

Surgical trauma to the fat itself also alters its local phenotype and can yield a systemic response in distal adipose depots[10]. In mice, unilateral surgical trauma to inguinal adipose tissue induces local and distal browning[11], but whether this is a beneficial adaptation to surgical stress is unknown. In the same model, reducing dietary fat intake for the 3 weeks leading up to the surgical injury not only reduced baseline levels of CCL2 and tumor necrosis factor-α (TNF-α), but also dampened the adipose tissue inflammatory response to surgical trauma[10].

This concept of utilizing short-term dietary interventions for surgical preconditioning stands as an emerging approach to enhance surgical outcomes[12,13]. Dietary restriction (DR), defined as restriction of either total calories, macronutrients, or specific amino acids, represents one such dietary preconditioning approach[13,14]. Efficacy of these short-term diets has been shown in a wide range of preclinical surgical models, including renal[12,15,16], hepatic[12,17,18] and vascular injury models[19]. Recently, we reported[20] that short-term dietary protein restriction limits adverse vascular remodeling in a murine venous bypass graft model via increased endothelial expression of cystathionine gamma-lyase. Induction of this transsulfuration enzyme results in increased endogenous production of the gaseous vasodilatory and anti-inflammatory molecule hydrogen sulfide[18]. Hydrogen sulfide in turn can function as a DR-mimetic when delivered via a locally applied gel during vein graft surgery, thereby limiting adverse vein graft remodeling[21].

Methionine restriction (MetR) is a DR regimen in which dietary sulfur amino acid (methionine and cysteine) content, but not overall calorie intake, is reduced. In rodents, MetR shows pleiotropic benefits on cardiometabolic health[22] and lifespan[23] likely via effects on adipose tissue[24] and energy metabolism[25,26]. In surgical models, MetR improves femoral ligation outcomes by increasing angiogenic potential[27] without detrimentally affecting wound healing[28]. In humans, MetR delivered for up to 16 weeks as a semi-synthetic diet is feasible and increases fat oxidation and reduces intrahepatic lipid content[29].

Here we tested the hypothesis that short-term preoperative MetR can attenuate adverse vascular remodeling in models of arterial injury and vein graft surgery specifically via interplay with PVAT, with implications for dietary preconditioning in human vascular injury. Mechanistically, we evaluated changes in PVAT gene expression prior to and after surgery and their modulation by MetR via bulk and single nucleus RNA sequencing.

Results

Protection from adverse vein graft remodeling via short-term methionine restriction is PVAT dependent

We first asked whether preconditioning with MetR could improve vein graft durability. Mice were subjected to a run-in period of 3 weeks with 60% fat, 0% cysteine diet (Control) with standard levels of methionine (0.6% of diet mass, 2.6% of total protein). Following run-in, one cohort was switched to a MetR diet containing 60% fat, 0% cysteine and low methionine (0.07% diet mass, 0.3% of total protein) (Fig. S1A). After 1 week of MetR or Control diet, mice were underwent a surgical intervention and were returned to Control diet immediately postoperatively (Fig. 1A). During the dietary intervention, mice on MetR lost 12% of their starting weight (Fig. S1B), despite hyperphagia (Fig. S1C), but regained weight rapidly postoperatively (Fig. S1B).

In the first experiment, mice underwent vein graft surgery[30] including partial stripping of venous PVAT (Fig. S2A)[31]. Caval veins from donor mice on matched diets to recipients were implanted in recipients. At POD28, vein grafts were harvested and processed for histology (Fig S2B). Histomorphometric analysis revealed that mice precondition with MetR had a significant decrease of 31% and 30.5% in I/M area and thickness ratios respectively (Fig. S2C, D).

We next sought to better understand the mechanism by which MetR protects against adverse vein graft remodeling. Considering the potential of PVAT to modify surgical outcome[9,10], together with the published effects of MetR on adipose tissue[24], we hypothesized that protection by short-term MetR is dependent on modulation of local PVAT. For this experiment, the donor caval vein was either stripped of PVAT ("No PVAT") or PVAT was left intact ("PVAT") before transplantation into a recipient on a matched diet, thus creating a vein graft without PVAT (Fig. 1B, C) or completely intact PVAT (Fig. 1D, E). Histomorphometric analysis at POD28 (Fig. 1F) revealed a PVAT-dependent protection from adverse remodeling by MetR, as demonstrated by a significant decrease in I/M area ratios (53%, Fig. 1G), and I/M thickness ratios (53%, Fig. 1H) compared to Control + PVAT. There was no difference between diet groups without PVAT. Furthermore, two-way ANOVA showed a significant diet−PVAT interaction effect in both vein graft layer thickness and area ratios (Fig. 1G, H). MetR + PVAT vein grafts trended toward a smaller intimal area (Fig. S3A) but there was no change in intimal thickness (Fig. S3B). At POD28, lumen area was decreased in MetR + PVAT mice (Fig. S3C). The favorable morphology of MetR + PVAT vein grafts was mainly driven by an increase in media thickness, (37%, Fig. 1I) and area (27%, Fig. 1J). All data on the interaction between diet and PVAT on histomorphometric parameters are summarized in Table 1.

Finally, we examined whether MetR could decrease IH induced by the creation of a focal stenosis in the right common carotid artery (RCCA) (Fig. S4A). Control mice exhibited adverse arterial remodeling and IH after focal stenosis, while preconditioning with MetR prevented IH at POD28 (Fig. S4B, C).

Short-term MetR modulates caval vein PVAT toward an arterial-like phenotype

We next performed a series of bulk transcriptomic analyses on PVAT to determine the effects of diet on transcriptional profiles before and after surgery (Fig. 2A). We focused on early timepoints to test the hypothesis that a diet by PVAT interaction was present before surgery and capable of modulating the early vein graft remodeling responses. Thoracic aorta PVAT from Control and MetR mice was also sequenced to investigate differences in venous (caval vein) vs. arterial (thoracic aorta) PVAT responses.

At baseline, venous and arterial PVAT from Control mice showed robust differences (4568 differentially expressed genes, Fig. S5A, B). Pathway analysis of differentially expressed genes revealed a brown-adipose tissue (BAT)-like phenotype in arterial PVAT, with increased peroxisome proliferator-activated receptor (PPAR*)* and *thermogenesis* signatures (Fig. 2B). In arterial PVAT, MetR modified expression of 1316 genes (Fig. S5C) and further induced PPAR and *thermogenesis* pathways (Fig. 2B) compared to Control mice.

In venous PVAT, MetR drove differential expression of 811 genes (Fig. S5D), which were enriched for PPAR signaling and fatty-acid biosynthesis (Fig. 2B). This transcriptomic profile, although not completely identical to arterial PVAT, did reveal increases in key pathways involved in browning. Thus, MetR drove a transcriptional signature of browning in both venous and arterial PVAT.

Analysis of venous PVAT at POD1 revealed vein graft surgery as a much larger modulator of gene expression than diet (Fig. S6A), with 4183 significantly differentially expressed genes vs. preoperative venous PVAT (Fig. S6B). These genes were mainly involved in innate and adaptive immune responses (Fig. 2C). Within POD1 PVAT, diet drove differential expression of 91 genes (Fig. S7B), which were also primarily involved in regulation of immune function (Fig. 2C). Interestingly, multiple pathways showed significant diet by surgery interaction effects (Fig. 2C).

https://doi.org/10.1038/s41467-024-53844-8

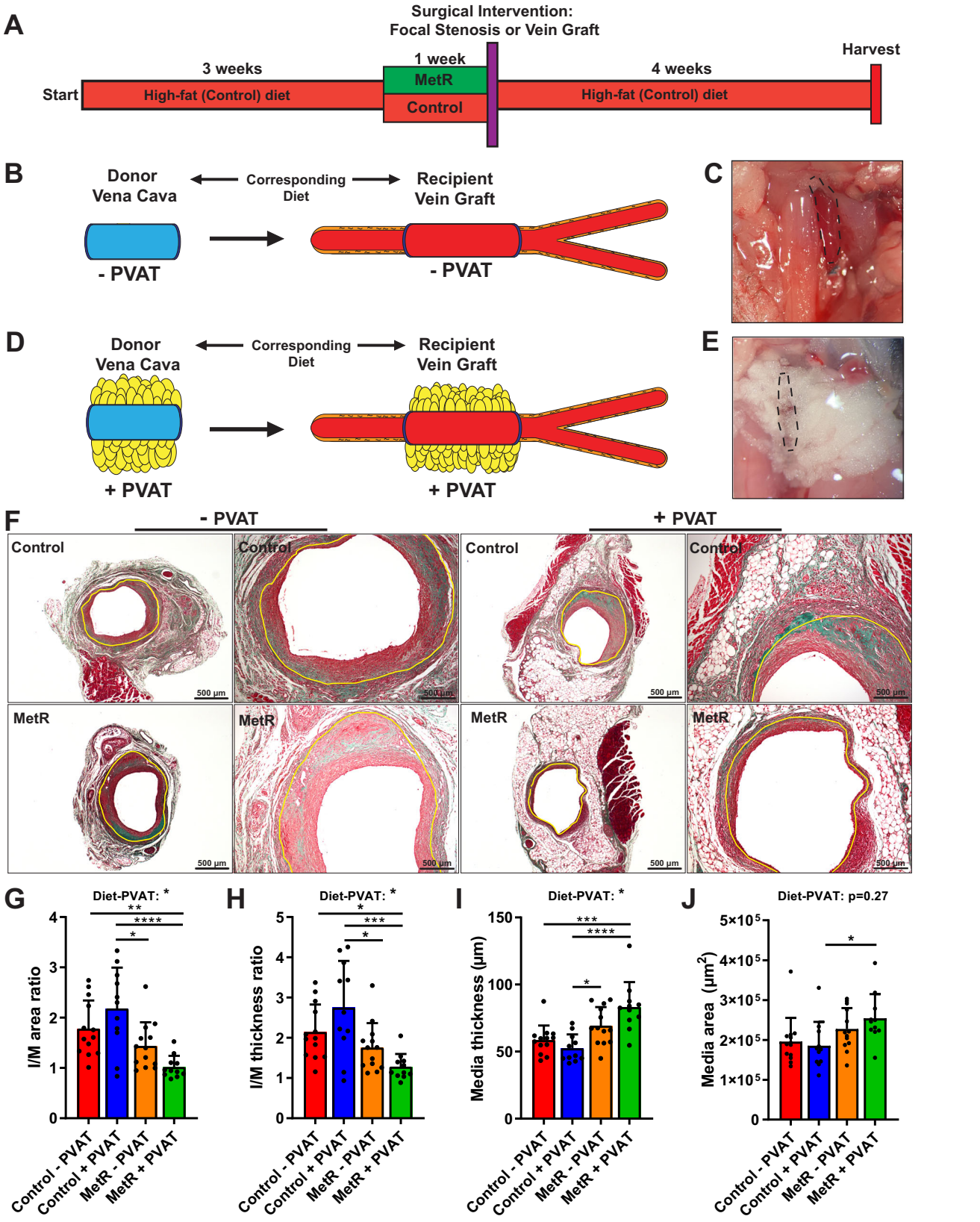

These pathways were primarily involved in immune function (hematopoietic cell lineage, B-cell receptor signaling, primary immunodeficiency) and lipid- and steroid hormone biosynthesis (Fig. 2C), suggestive of a diet-dependent immune response to surgical stress. In line with these findings, we observed a dampening of toll-like receptor 4 (*Tlr4*) gene expression (Fig. S6C) together with a robust decrease in expression of its endogenous ligand[32] tenascin-C (Fig. S6D) in the MetR group following surgery. Lysyl-oxidase[33] (*Lox*), an enzyme involved in atherogenesis and restenosis, was also strongly downregulated in MetR PVAT at POD1 (Fig. S6E). The decrease in expression of *Lox* and *Tnc* in MetR PVAT at POD1 was confirmed by qPCR (Fig. S6F, G).

Fig. 1 | Protection from adverse vein graft remodeling via short-term methionine restriction is perivascular adipose tissue dependent. A Schematic overview of dietary intervention. **B**–**E** Schematic and in-situ images of vena cava/vein graft ± PVAT. **B**, **C** Stripping of venous PVAT results in vein graft lacking PVAT. **D**, **E** Vena cava with PVAT and consecutive vein graft with PVAT intact. **F** Images of vein grafts at POD28 after Masson-trichrome staining. Control and MetR, no PVAT or PVAT. Scale bars = 200 or 500 μm as indicated. **G**–**J** Histomorphometric analysis of POD28 vein grafts (Control − PVAT $n = 13$, Control + PVAT $n = 11$, MetR − PVAT $n = 13$, MetR + PVAT $n = 11$). **G** I/M area ratio (*$p = 0.0108$, **$p = 0.0084$). **H** I/M thickness ratio (Control − PVAT vs. MetR + PVAT $p = 0.0403$; Control + PVAT vs. MetR − PVAT $p = 0.0313$; ***$p = 0.0006$). **I** Media thickness (*$p = 0.0223$, ***$p = 0.0004$). **J** Media area (*$p = 0.0385$). All statistical testing was done via two-way ANOVA with Tukey's multiple comparisons test unless otherwise indicated. Graphs are presented as mean ± SD *$p < 0.05$, **$p < 0.01$, ***$p < 0.001$, ****$p < 0.0001$. Source data are provided as a Source Data file.

Table 1 | Percentage of variation between groups that can be explained by diet, PVAT or a diet–PVAT interaction

Histomorphometric parameter	Source of variation	% of total variation	p value	p value summary
I/M area ratio (Fig. 1G)	Interaction	9.146	0.0146	*
	PVAT +/−	0.006033	0.9482	ns
	Diet	31.16	<0.0001	****
I/M thickness ratio (Fig. 1H)	Interaction	7.538	0.0324	*
	PVAT +/−	0.001153	0.9783	ns
	Diet	24.40	0.0003	***
Intimal area (Fig. S3A)	Interaction	4.274	0.1451	ns
	PVAT +/−	0.3439	0.6760	ns
	Diet	10.96	0.0219	*
Media area (Fig. 1J)	Interaction	2.284	0.2734	ns
	PVAT +/−	0.4127	0.6397	ns
	Diet	16.50	0.0047	**
Intimal thickness (Fig. S3B)	Interaction	2.507	0.2736	ns
	PVAT +/−	1.591	0.3819	ns
	Diet	6.780	0.0751	ns
Media thickness (Fig. 1I)	Interaction	8.223	0.0159	*
	PVAT +/−	1.254	0.3325	ns
	Diet	35.61	<0.0001	****
Lumen area (Fig. S3C)	Interaction	6.514	0.0719	ns
	PVAT +/−	0.2124	0.7407	ns
	Diet	10.26	0.0253	*

Two-way ANOVA with Tukey's multiple comparison test on histomorphometric parameters in Fig. 1 and Fig. S3.
*$p < 0.05$, **$p < 0.01$, ***$p < 0.001$, ****$p < 0.0001$.

Short-term MetR induces browning in venous PVAT associated with adipocyte-specific PPAR-α activation and dampens post-operative pro-inflammatory macrophage response

To determine which specific cell types in MetR-preconditioned PVAT are involved in thermogenic activation and immune response modulation, we performed single nucleus RNA sequencing on Control and MetR preconditioned venous PVAT at baseline and at POD1. Figure S7A–C demonstrates technical validity of the sequencing, with low per-sample and inter-sample variability. Both Control and MetR PVAT had a distinct UMAP cell clustering signature, both at the pre-operative and POD1 timepoint (Fig. 3A, B). We identified robust marker genes for each cluster with limited redundancy between clusters (Fig. S8AC). Cell type identity for each cluster was assigned using canonical marker genes (Fig. S8B) which was validated using an unbiased comparison to reference datasets (Fig. S7D).

Preconditioning with MetR resulted in pronounced changes in transcriptional profiles in several PVAT cell types (Fig. 2D, E), including mesenchymal (cluster 0) and stromal cells (cluster 3). The greatest preoperative signature change after MetR however, was seen in adipocytes to the extent that they were classified into distinct clusters (clusters 8, 9). In preoperative PVAT adipocytes (Fig. S8F), several pathways involved in energy- and fatty-acid metabolism were significantly enriched in genes increased by MetR (Fig. 2F). Notably, there was marked increased expression of *Ppara* and several related thermogenic genes, and this effect was confined to MetR preconditioned preoperative PVAT adipocytes (Fig. 2G).

At the POD1 timepoint, several clusters showed distinct transcriptional signatures induced by diet (Fig. 2D, E), including fibroblasts (clusters 1, 2), adipocytes (cluster 7) and macrophages (cluster 10). In postoperative macrophages (Fig. S8G), genes increased by MetR preconditioning were significantly enriched for pathways involved in translation and formation of extra-cellular matrix (Fig. 2H). Individual transcripts that were shown to be highly regulated by MetR in postoperative macrophages were mainly associated with an anti-inflammatory macrophage phenotype, such as *Malat1*[34] and *Cebpd*[35] (Fig. 2I). Interestingly, PPAR-α regulation was no longer present in MetR POD1 PVAT adipocytes, but rather MetR induced upregulation of several pathways involved in extra-cellular matrix remodeling and protein synthesis at POD1 (Fig. S8H).

Collectively, these data suggest that adipocyte PPAR-α induction by MetR may induce an "arterial-like" phenotype in preconditioned venous PVAT. Interestingly, PPAR-α expression was no longer increased at POD1. Alternatively, in macrophages no baseline effect was evident, however, at POD1 MetR preconditioning drove a marked anti-inflammatory phenotype.

Short-term MetR induces browning in venous PVAT which is sustained until POD28

Because MetR modulated PPAR signaling in venous PVAT, we also investigated specific genes involved in browning. *Ucp1* showed a significant diet effect across preoperative and postoperative timepoints with expression increased by MetR (Fig. 3A). We also observed a significant diet effect on *Ppara* expression, though with smaller effects than *Ucp1* (Fig. 3B). Expression of *Leptin* was also significantly decreased as a function of MetR diet across timepoints (Fig. 3C). Immunohistochemical staining in POD1 vein grafts confirmed the transcriptional effects on *Ucp1* were confirmed using immunohistochemical staining in POD1 vein grafts, where we observed an increase in UCP1 protein levels (159% increase, Fig. 2D, E). Moreover, in POD28 vein grafts, we detected an increase in both UCP1 protein levels (77% increase, Fig. 2F, G) and a decrease in adipocyte size[36] (Fig. 3H). PPAR-α protein expression did not differ at this late-stage remodeling timepoint (Fig. 3I).

Altogether, these data substantiate our bioinformatical observations that MetR induces browning in venous PVAT. Moreover, the increased UCP1 protein levels at POD1 vein grafts suggest that this response is sustained after bypass surgery, whilst the smaller adipocyte size and increased UCP1 expression at POD28 suggest that the response is maintained until at least 28 days after surgery.

MetR activates PPAR-α signaling in adipocytes and dampens the inflammatory response of macrophages and PVAT in vitro and ex vivo

To assess the direct effect of MetR on secretion of pro-inflammatory cytokines by PVAT, we incubated venous PVAT ex vivo in either Control or MetR culture medium (Fig. 4A) and found decreased secretion of IL-6 (Fig. 4B), CCL2 (Fig. 4C) and TNF-α (Fig. 4D) in the supernatant

https://doi.org/10.1038/s41467-024-53844-8

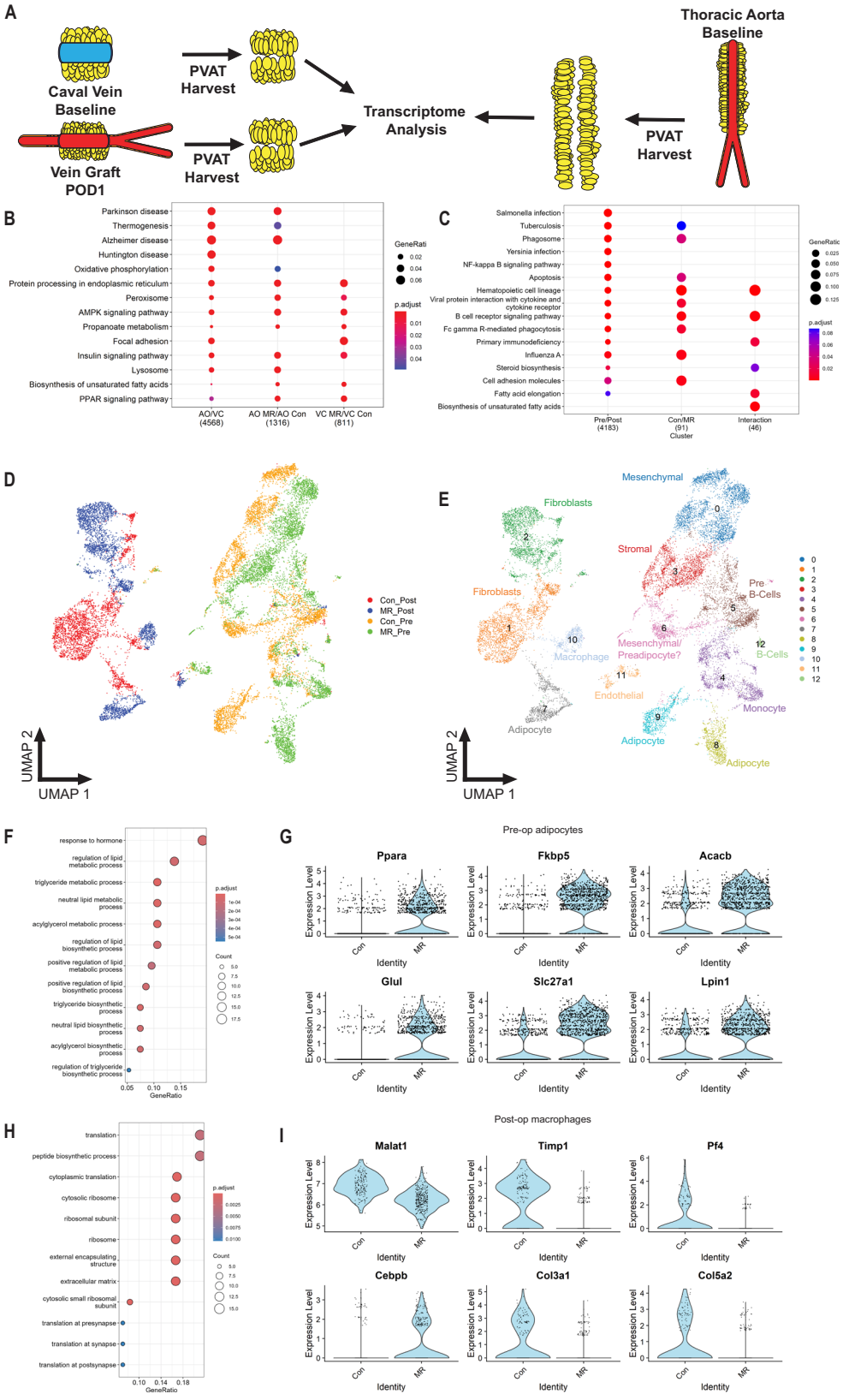

of MetR preconditioned PVAT, confirming a direct anti-inflammatory effect of MetR in PVAT.

Next, we cultured bone marrow-derived macrophages (BMDM) from C57BL/6J mice and stimulated them with LPS to induce a pro-inflammatory phenotype (Fig. 4E). Thereafter, we subjected them to various concentrations of MetR to determine effects on pro-inflammatory macrophages. The excretion of IL-6 (Fig. 4F) and TNF-α (Fig. 4G), but not CCL2 (Fig. 4H) was diminished upon MetR incubation. Interestingly, *Arg1* (Fig. S9A, anti-inflammatory macrophage marker[37]) was still modestly downregulated, and we did not find any difference in *Tnfα* and *Il6* gene expression (Fig. S9B, C). There was, however, a strong decrease in *Ccr2* (Fig. 4I), *Cd38* (Fig. 4J, pro-

Fig. 2 | Short-term MetR modulates caval vein PVAT toward an arterial-like phenotype. Bulk RNA sequencing (**A**–**C**) was performed on IVC and vein graft POD1 PVAT in Control and MetR mice ($n = 5$/group). Similarly, single-cell nuclear sequencing (**D**–**I**) was performed on IVC and vein graft POD1 PVAT in Control and MetR mice ($n = 2$/group). **A** Schematic of venous (preoperative and POD1) PVAT; and of thoracic aorta PVAT harvest, three separate adipose tissue depots processed for transcriptome analysis simultaneously. **B** Pathway analysis of thoracic aorta vs. venous (preoperative) PVAT of Control mice (AO/VC, first column), thoracic aorta PVAT MetR vs. Control (AO MR/AO Con, second column) and venous PVAT MetR vs. Control (VC MR/ VC Con, third column). **C** Pathway analysis of vein graft PVAT at POD1, MetR vs. Control. **D** UMAP project of cells colored by diet/surgery group. $N = 2$/group (Con/MR Control/MetR and Pre/Post preoperatively/postoperatively). **E** UMAP projection of cells colored by cluster with cell type description. $N = 2$/group **F** Pathway analysis of top 100 differentially expressed genes in preoperative adipocytes between Control and MetR groups. **G** Violin plots of top differentially expressed genes in preoperative adipocytes. **H** Pathway analysis of top 100 differentially expressed genes in postoperative macrophages between Control vs. MetR. **I** Violin plots of top differentially expressed genes in postoperative macrophages. **B**, **C**, **F**, **H** Gene set over-representation analysis with false detection rate correction.

inflammatory macrophage marker[38]) and *Gpr18* expression (Fig. 4K, pro-inflammatory macrophage marker[39]) compared to Control medium, suggesting a diminished pro-inflammatory response after LPS stimulation.

Third, we sought to test PPAR-α activation in adipocytes in vitro using a 3T3-L1 adipocyte cell line. Incubation of differentiated 3T3-L1 adipocytes with MetR-medium (Fig. 4L) induced a significant increase in the expression of *Ppara* (Fig. 4M).

Lastly, we assessed a potential causal relationship between the upregulation of *Ppara* in adipocytes and the diminished pro-inflammatory response macrophages in PVAT. We cultured adipocytes and macrophages separately whilst subjecting either adipocytes or macrophages to MetR, followed by a co-culture experiment with both cell types in a transwell system. Macrophages that were stimulated with LPS and subjected to MetR, did not increase *Ppara* expression in adipocytes. Conversely, preconditioning of adipocytes with MetR did dampen the pro-inflammatory activity of macrophages, as is shown via decreased production of CCL2 (Fig. 4Q, significant) and IL-6 (Fig. 4R, non-significant), whilst TNF-α was not excreted (Fig. S9D). Additionally, we confirmed these results on a transcriptional level in macrophages with decreased gene expression of *Ccl2* (Fig. 4S), but not *Il6* (Fig. 4T).

In summary, MetR reduced the excretion of pro-inflammatory cytokines by caval vein PVAT in vitro. Specifically, we observe dampened pro-inflammatory responses by BMDMs as a result of MetR. Moreover, MetR unidirectionally activates adipocytes to trigger an anti-inflammatory response in macrophages in vitro, which aligns with our in vivo nuclear sequencing data in vein graft PVAT macrophages.

The MetR PVAT interaction in vivo promotes an anti-inflammatory macrophage phenotype

To better understand whether any of our baseline and POD1 findings in macrophages and adipocytes associate with a favorable late-stage remodeling, we assessed vein grafts at POD28. In the MetR + PVAT group, reduced pro-/anti-inflammatory macrophage ratios were observed both in the graft wall (Fig. 5A, C) and PVAT (Fig. 5B, C). The favorable ratio observed in both vein graft layers was driven by a significant interaction between MetR and the presence of PVAT (Fig. 5A and Table 2). The observed differences in ratios could be explained by increased polarization toward the anti-inflammatory phenotype, both in the intimal and media layers (Fig. 5D) and in MetR PVAT (Fig. S10A), while there was a limited decrease in pro-inflammatory macrophages in the vein graft wall (Fig. 5E) and PVAT (Fig. S10B). Preconditioning with MetR yielded no difference in total macrophages in the vein graft wall (Fig. S10C), nor in surrounding PVAT (Fig. S10D). This increase in intimal anti-inflammatory macrophages together with an apparent small decrease in pro-inflammatory macrophages in the MetR + PVAT cohort could also be linked to the underlying interplay between diet and PVAT (Fig. 5D, E and Table 2).

Differences in the percentage of intimal area and whole vein graft occupied by VSMC were dependent on the interaction between diet and PVAT at POD28 (Fig. 5F, G and Table 3), but no significant difference in directionality could be detected between groups. The absolute number of VSMC per mm^2 present was similarly dependent on a diet by PVAT interaction, but this effect was not strong enough to display significant inter-group differences (Fig. S10E and Table 3). There was no detectable change in proliferating VSMC at POD28 (Fig. 5G and Table 3), nor did extra-cellular matrix analysis reveal a change in collagen deposition (Fig. S10F and Table 3).

In summary, our data revealed that short-term preconditioning with MetR drove venous PVAT toward a more arterial-like state by induction of browning and *Ppara* in PVAT adipocytes. This transition to a more arterial-like transcriptional profile was accompanied by early anti-inflammatory responses in PVAT-macrophages and resulted in beneficial late-stage vein graft remodeling including improved pro-/anti-inflammatory macrophage ratios (Fig. 6A–C).

Discussion

Here we tested the potential of short-term restriction of the sulfur amino acids methionine and cysteine (MetR) in preclinical models of cardiovascular surgery interventions. Excitingly, just 1 week of the MetR intervention, which constitutes an isocaloric diet with adequate levels of all macronutrients, protected from arterial IH in a focal stenosis model, and protected from adverse remodeling after vein graft surgery. Specifically in bypass surgery, we show that protection from MetR was entirely dependent on the presence of PVAT. Control mice who received a caval vein with intact PVAT had exacerbated vein graft disease (VGD) at POD28, pointing toward a diet-induced reversal of PVAT phenotype in MetR mice compared to Control diet. There were no significant histomorphometric differences detectable between diet groups when caval veins were stripped of PVAT before anastomosis creation, indicating a PVAT-dependent protection from negative remodeling by MetR.

In this study, we performed a side-by-side comparison of arterial (thoracic aorta) and venous (caval vein) PVAT via bulk RNA sequencing, while also examining the effects of MetR and surgical stress on the PVAT transcriptome. Our study revealed distinct transcriptomic profiles between caval vein and thoracic aorta PVAT, with caval vein PVAT resembling white/beige adipose tissue[40]. Thoracic PVAT resembled BAT, with increased expression of thermogenic genes[41]. Interestingly, short-term MetR further increased browning in arterial (thoracic aorta) PVAT, while it induced this phenotype in venous (caval vein) PVAT. Single nucleus sequencing and ex vivo/in vitro experiments confirmed that this is likely a direct effect of MetR on PVAT adipocytes. While it is known that long-term (weeks–months) MetR induces browning in inguinal beige adipose tissue[25,42,43], here we were able to induce this phenotype in venous PVAT after just 1 week of MetR. Moreover, the similar transcriptomic response in both arterial (thoracic aorta) and venous (caval vein) PVAT suggests that MetR-induced browning does not depend on PVAT origin, which should, however, be confirmed in future studies. Furthermore, MetR responses are highly sexually dimorphic, with females showing resistance to MetR metabolic benefits, which includes browning of adipose tissue[44,45]. Whether this also applies to PVAT is currently unknown. The use of male mice in this study is a major limitation and our findings may not represent the biology of women. Future research should thus

https://doi.org/10.1038/s41467-024-53844-8

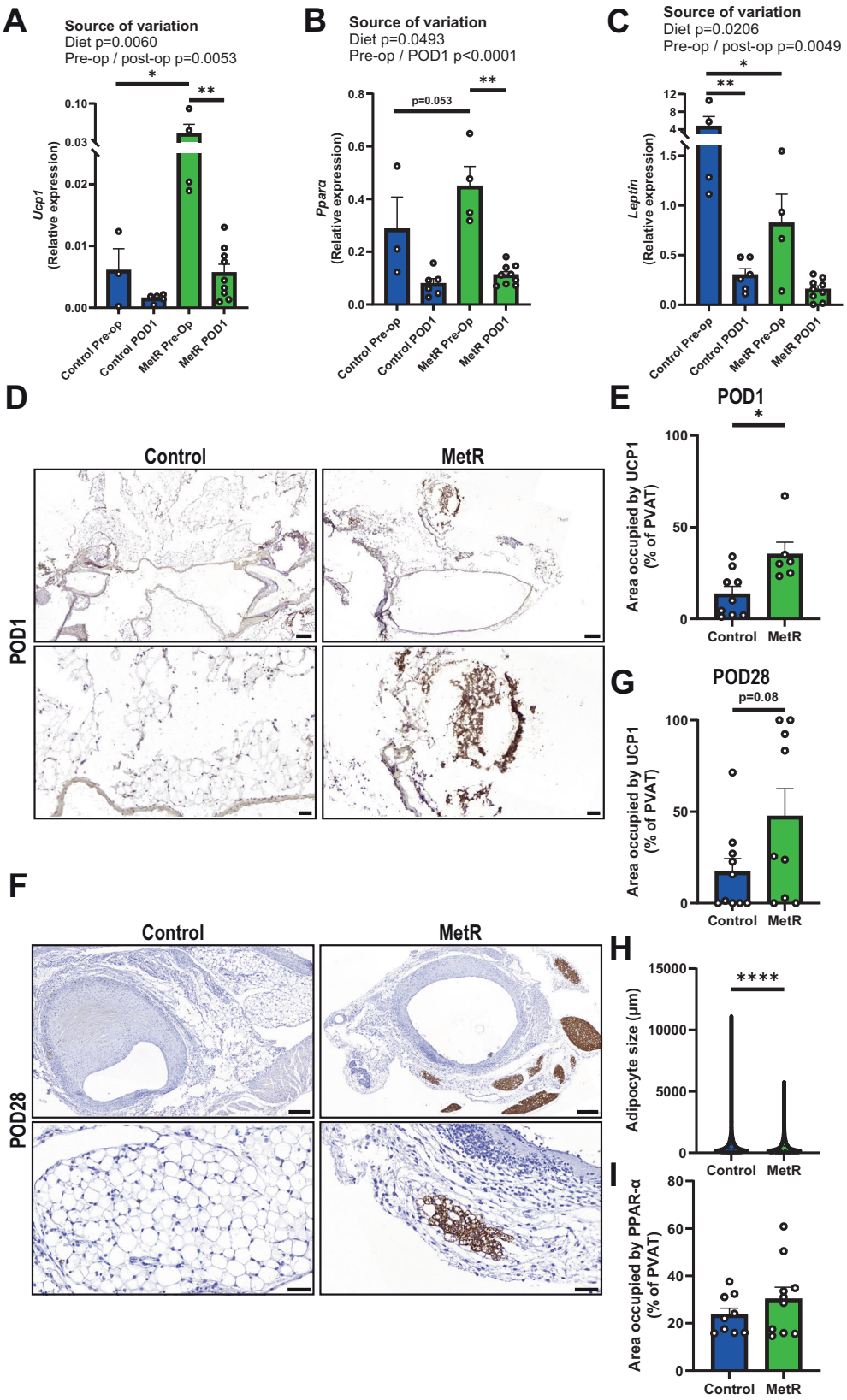

optimize a female-specific MetR paradigm to allow replication of these findings in female mice

In addition to bulk RNA sequencing, we also performed single nucleus RNA sequencing of PVAT. Our analysis revealed that browning of PVAT coincided with the increased expression of *Ppara* specifically in adipocytes upon MetR, which corroborates evidence from previous studies on long-term MetR in inguinal adipose tissue[25,46]. This signature was transient and not present in POD1 PVAT adipocytes, therefore likely a direct result of MetR. It is likely that MetR induces *Ppara* locally and directly in PVAT adipocytes as we were able to replicate this in vitro in adipocytes under MetR conditions. A recent study by Decano et al.[47] revealed a novel and decisive role for PPAR-α in VGD,

Fig. 3 | Short-term MetR induces browning in venous PVAT which is sustained until POD28. A *Ucp1* (*$p = 0.0158$, **$p = 0.0018$), **B** *Pparα* (***$p = 0.0002$) and **C** *Leptin* gene expression in preoperative and POD1 PVAT (*$p = 0.0407$, **$p = 0.0076$), all tested via Two-way ANOVA with Bonferroni's multiple comparisons test (Control preoperative $n = 3$, Control POD1 $n = 5$, MetR preoperative $n = 4$, MetR POD1 $n = 9$). **D** Images of UCP1 stained vein grafts at POD1 in both Control and MetR-preconditioned mice, scale bars = 200 μm (overview) or 50 μm (zoom-in). **E** Quantification of UCP1 positive cells after IHC in PVAT of vein grafts at POD1 ($p = 0.0116$, Control $n = 9$, MetR $n = 6$). **F** Images of UCP1 stained vein grafts at POD28 in both Control and MetR-preconditioned mice, scale bars = 200 μm (overview) or 50 μm (zoom-in). **G** Quantification of UCP1 positive cells after IHC in PVAT of vein grafts at POD28 ($p = 0.0776$, Control $n = 10$, MetR $n = 9$). **H** individual adipocyte size in vein grafts at POD28 in both Control and MetR-preconditioned cohorts. **I** Quantification of PPAR-α positive cells after IHC in PVAT of vein grafts at POD28 (Control $n = 9$, MetR $n = 10$). All statistical testing was done via unpaired *t*-test unless otherwise indicated. Graphs are presented as mean ± SEM. *$p < 0.05$, **$p < 0.01$, ***$p < 0.0001$ ****$p < 0.0001$. Source data are provided as a Source Data file.

demonstrating prevention of graft failure by PPAR-α activation specifically in macrophages, which muted their pro-inflammatory capabilities. Additionally, another recent study associated loss of PPAR-α with negative vein graft remodeling by differentiation of PVAT-derived mesenchymal stem cells into SMCs which contribute to IH, pointing toward a pivotal role of PPAR-α signaling in various cell types[48]. Our results suggest that PPAR-α may also play a protective role in PVAT adipocytes, strengthening the evidence for an overall beneficial role of PPAR-α signaling within the vein graft microenvironment.

In addition to direct action on adipocytes, it is also possible that PVAT browning is induced via distal signaling in response to MetR. Previous studies show that MetR drives hepatic production of fibroblast growth factor-21 (FGF-21)[49], a hormone directly responsible for the regulation of *thermogenesis* in both white and brown adipose depots[50]. In the current study, we subjected both donor and recipient to MetR before vein graft surgery, leaving open the possibility that MetR induces PVAT browning via both direct action on PVAT adipocytes in the donor, and increased hepatic FGF-21 production in the recipient[50].

One week of MetR diet drove an ~10% reduction in body weight despite significantly increased energy intake. This finding is consistent with previous studies which show that MetR-induced weight loss is driven by increased energy expenditure rather than reduced energy intake[22,44,45]. While we cannot fully rule out that part of the diet-induced benefit is driven by energy deficit, our results do suggest that dietary energy restriction per se is not required for presurgical protection. Supporting this finding, direct comparisons of MetR and calorie restriction reveal distinct effects on metabolic and inflammatory transcriptomic profiles in liver[51], suggesting distinct causal mechanisms between calorie restriction and MetR.

Transcriptomic responses to surgery were much larger than diet at the POD1 timepoint, which is logical considering the severe changes in environment and stressors that veins undergo when switched to an arterial circulation[4]. We noted strong activation of several pathways involved in the immune response, which confirms previous findings in vein grafts regarding the involvement of immune cells in early remodeling stages[52–54]. Single-cell analysis of vein graft PVAT at POD1 revealed a marked shift in macrophages toward an anti-inflammatory phenotype after MetR, including reduced *Malat1* and *Timp1* expression. This also appears to be a direct effect, as in vitro MetR culture shifted macrophages toward an anti-inflammatory phenotype and reduced the production of pro-inflammatory cytokines IL-6 and TNF-α. In addition, analysis of vein grafts at POD28 revealed a marked shift in macrophage polarization toward an anti-inflammatory phenotype in the MetR + PVAT group, and this was dependent on the diet–PVAT interaction.

In adverse vein graft remodeling, macrophages function as one of the main effector cells in the cascade ultimately leading to graft occlusion[4], and the presence of anti-inflammatory macrophages in grafts is associated with favorable remodeling outcomes[30]. When methionine is in abundance, macrophages progress toward a pro-inflammatory phenotype[55], but here we show a robust reversal when methionine is restricted. Increased polarization of macrophages toward an anti-inflammatory phenotype is associated with low levels of TIMP-1[56], while *MALAT1* is a long-coding RNA[34] that recently has been inversely correlated with in-stent stenosis after coronary revascularisation[57].

MALAT1 may function as a negative feedback sensor for the activation of the TLR4 pathway in macrophages in response to endogenous or exogenous ligands[58]. Whether MetR directly downregulates *Malat1* or that this is merely a result of decreased activation of pro-inflammatory pathways (such as TLR4) in macrophages preconditioned with MetR is unknown. Interestingly, our whole-transcriptome data reveal marked downregulation of *Tlr4* and the TLR4 ligand tenascin-C, suggesting the latter. In the context of adverse vein graft remodeling, deficiency of TLR4 is directly linked to a decrease in adverse graft wall remodeling[30,59]. Our in vitro experiments demonstrate that this macrophage shift toward an anti-inflammatory state is derived from a cell autonomous response to MetR as well as paracrine signaling by adipocytes. Conversely, macrophages preconditioned with MetR did not induce browning in adipocytes which excludes induction of browning in adipocytes via MetR preconditioned macrophages.

In (coronary) bypass surgery, PVAT has been previously studied regarding the "no touch" technique. In this approach, the vein graft is transplanted with its PVAT intact to potentially improve graft patency[6,60,61]. Recently, several trials in humans have been conducted but with conflicting results. A 2019 trial by Deb et al. was not able to find any differences in patency rates between groups[62], while a 2021 trial by Tian et al. did report over 40% reduction in vein graft occlusion in the no-touch group[63]. In a study performed by Deb et al., average BMI in both groups was 28–29, while Tian et al. noted significantly diminished patency rates in high-BMI (>25) cohorts after sub-group analysis.

High-fat feeding and subsequent obesity exert detrimental effects on PVAT adipocytes and vascular function[7,64–66]. Specifically in cardiovascular surgery models, high-fat feeding exacerbates IH after vascular injury via pro-inflammatory changes in PVAT[8,9,67]. Extrapolating these findings to the aforementioned clinical trials, BMI may explain outcome discrepancies as a proxy for the presence of an unfavorable PVAT phenotype. In our study, we also noticed detrimental effects on PVAT-phenotype and subsequential vein graft remodeling after (prolonged) Control-diet high-fat feeding, most likely as a result of increased inflammation, but this was completely reversed by short-term MetR compared even to MetR without PVAT.

In summary, we demonstrate that short-term preconditioning with MetR reduces VGD in a PVAT-dependent manner. These effects were associated with an induction of browning in PVAT and a shift in vein graft macrophages toward an anti-inflammatory phenotype. MetR represents a simple, low-cost dietary intervention which is feasible and safe in humans[29]. Our study demonstrates the promising potential of MetR for improving PVAT phenotype and subsequent vascular surgery outcomes. Future work may aim to evaluate the effects of MetR preconditioning on vascular remodeling outcomes in powered human cohorts.

Methods

Experimental animals

All animal experiments were approved by the appropriate Brigham and Women's Hospital Institutional Animal Care and Use Committee and

https://doi.org/10.1038/s41467-024-53844-8

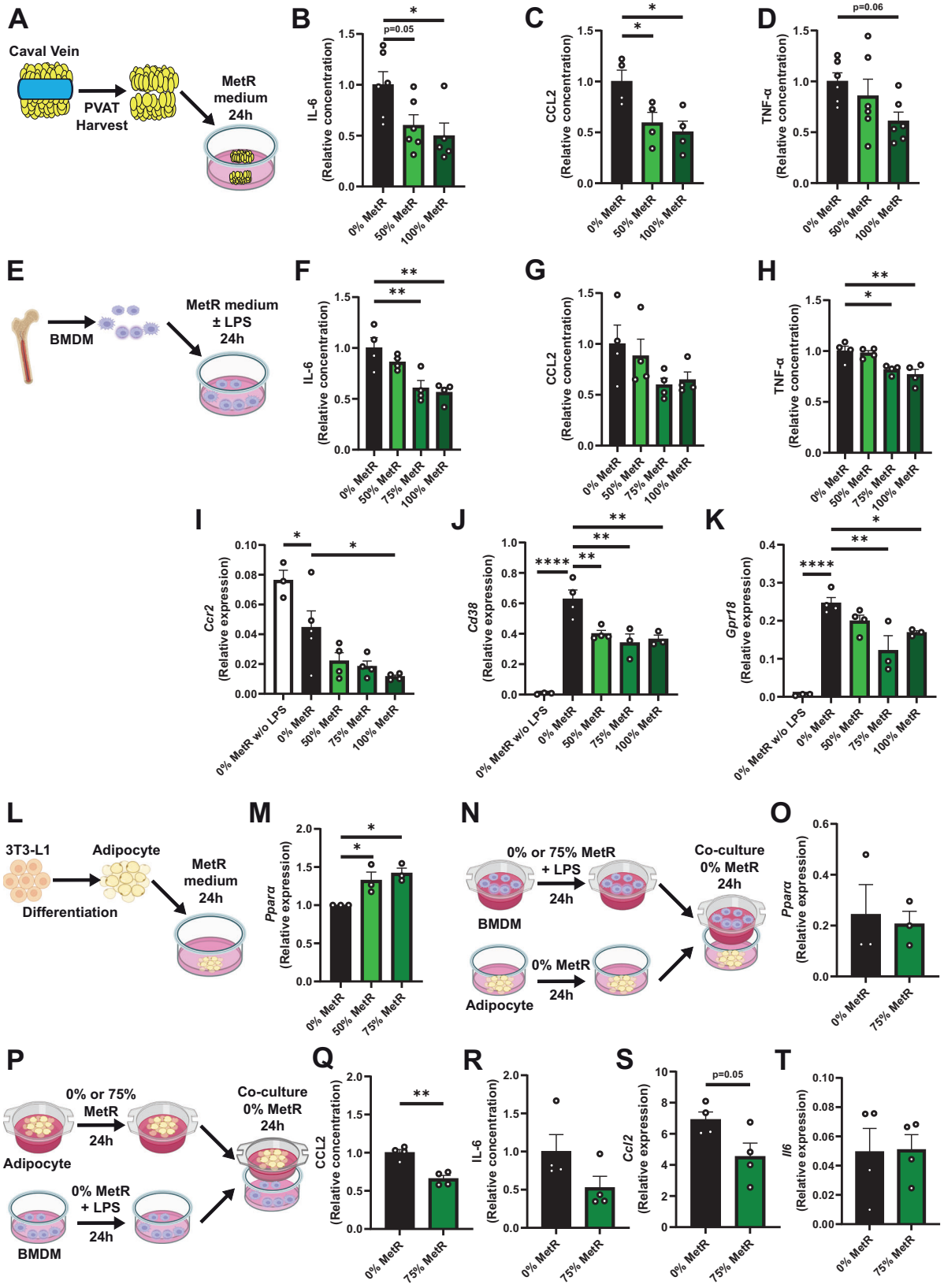

performed in accordance with the NIH recommendations for care. All surgical experiments were performed on HFD-fed C57BL/6J mice (male, 14–16 weeks old, Stock No: 380050, Jackson Laboratory). Male mice were used in this study due to our earlier findings that estrogen inhibits neointima formation[68], and previous work showing that MetR responses are highly sexually dimorphic, with females showing resistance to MetR metabolic benefits[44,45]. We recognize this as a limitation and future research should optimize a female-specific MetR paradigm to allow replication of these findings in female mice. Mice were housed 4–5 per cage and maintained on a 12-h light–dark cycle at 22 °C with 30–50% humidity. The diets (both MetR and control) were given ad libitum for the entire duration of the study, with mice having

Fig. 4 | MetR activates PPAR-α signaling in adipocytes and dampens the inflammatory response of macrophages and PVAT in vitro and ex vivo. **A**–**D** Venous PVAT was harvested from C57BL/6J mice and cultured in vitro. **A** Schematic overview of experimental setup. **B** IL-6, (*$p = 0.0220$, 0% $n = 6$, 50% $n = 6$, 100% $n = 5$) **C** CCL2 (0% vs. 50% $p = 0.0445$, 0% vs. 100% $p = 0.0176$, % 0% $n = 4$, 50% $n = 4$, 100% $n = 4$) and **D** TNF-α levels in supernatant of PVAT (0% $n = 6$, 50% $n = 6$, 100% $n = 6$). **E**–**K** Bone marrow-derived macrophages (BMDMs) were stimulated with LPS and incubated for 24 h in Control or MetR medium. **E** Schematic overview of experimental setup. **F** IL-6, (0% vs. 75% $p = 0.0048$, 0% vs. 100% $p = 0.0022$) **G** CCL2 and **H** TNF-α levels in the supernatant of BMDMs (*$p = 0.0166$, **$p = 0.0035$) (**F**–**H**; $n = 4$/group). **I** qPCR for *Ccr2*, (0% vs. 0% w/o LPS $p = 0.0370$, 0% vs. 100% $p = 0.0171$, 0% w/o LPS $n = 3$, 0% $n = 5$, 50% $n = 4$, 75% $n = 4$, 100% $n = 4$) **J** *Cd38* (****$p = 0.0001$, 0% vs. 50% $p = 0.0049$, 0% vs. 75% $p = 0.0015$, 0% vs. 100% $p = 0.0029$) and **K** *Gpr18* in pro-inflammatory macrophages under Control and MetR conditions (*$p = 0.0438$, **$p = 0.0020$) (**J**, **K**; 0% w/o LPS $n = 3$, 0% $n = 4$, 50% $n = 4$, 75% $n = 3$, 100% $n = 3$). **L**, **M** 3T3-L1 cells were differentiated to adipocytes and incubated for 24 h with Control or MetR medium. **L** Schematic overview of experimental setup. **M** qPCR for *Ppara* in 3T3-L1-differentiated adipocytes ($n = 3$/group). **N**–**T** Co-culture experiments. **N** Schematic overview of experimental setup. **O** qPCR for *Ppara* in adipocytes after 24-h incubation with BMDMs, tested via unpaired *t*-test (0% vs. 50% $p = 0.0341$, 0% vs. 75% $p = 0.0117$) ($n = 3$/group). **P** Schematic overview of experimental setup. **Q** CCL2 (**$p = 0.0014$) and **R** IL-6 levels in supernatant, tested via unpaired *t*-test. **S** qPCR for *Ccl2* and **T** *Il6* in BMDMs, tested via unpaired *t*-test (**P**–**T**; $n = 4$/group). **A**, **E**, **L**, **N**, **P** Created with BioRender.com, released under a Creative Commons Attribution-NonCommerical-NoDerivs 4.0 International License. All statistical testing was done via one-way ANOVA with Dunnet's multiple comparisons test, unless otherwise indicated. Graphs are presented as mean ± SEM. *$p < 0.05$, **$p < 0.01$, ****$p < 0.0001$. Source data are provided as a Source Data file.

unlimited access to the diet for 24 h/day. We and others have previously shown that MetR does not affect circadian patterns in food intake, energy expenditure or respiratory quotient[69,70]. The animal facility was specific pathogen-free (SPF) as confirmed by quarterly sentinel animal testing.

Dietary intervention

Upon arrival to the facility, all mice (aged 11–13 weeks old) were started on a 3-week 60% fat (by calories), 0% cysteine diet (Research Diets, A18013001) [Control] which contained standard levels of methionine (0.6% of energy, 2.6% of total protein). After 3 weeks of Control diet, 1 cohort was switched to a MetR diet containing 60% fat, 0% cysteine and 0.07% of energy from methionine (0.3% of total protein) [Research Diets, A18022602]. After 1 week of MetR or continued Control diet, mice were either harvested for baseline studies or underwent a surgical intervention. Immediately postoperatively, all mice were switched back to the Control diet and tissue was harvested at either POD1 or POD28 (Fig. 1A).

Vein graft surgery

Vein graft surgery was performed as described previously[30]. In brief, mice were anesthetized with isoflurane for the duration of the procedure. Shortly before the start of the recipient surgical procedure, the thoracic caval vein of a donor mouse on a matched diet was harvested and placed in sterile 0.9% NaCl supplemented with heparin (100 UI/mL). In the recipient, neck region fur was removed, and a neckline incision was performed. The RCCA was dissected from its surrounding soft tissues and two 8-0 nylon sutures were tied in the middle, ~1 mm apart. The RCCA was then cut between the two sutures to facilitate an end-to-end anastomosis. The proximal and distal RCCA was then everted over an autoclavable nylon cuff (Portex) of ~2 mm while clamped with vascular clamps. The everted carotid walls were secured with an 8-0 nylon suture. Next the donor caval vein was sleeved between both RCCA ends, and an end-to-end anastomosis was created with 8-0 nylon sutures. The distal followed by the proximal vascular clamp was released to restore blood flow. The incision was closed with 6-0 Vicryl sutures. Postoperatively animals received warm Ringer's lactate solution (0.5 mL, subcutaneous) and buprenorphine (0.1 mg/kg, subcutaneous).

Focal stenosis creation

A focal stenosis was created as described previously[71] to generate an arterial intimal hyperplastic response. Anesthesia was induced via 4% isoflurane and maintained via 2–3% isoflurane in a nose cone for the duration of the procedure. The RCCA was dissected from its surrounding tissue. A 35-gauge blunt needle mandrel was then placed longitudinally along the RCCA and tied with a 9-0 nylon suture ~2–2.5 mm proximal to the bifurcation. After removal of the needle mandrel, the skin was closed with a 6-0 Vicryl suture. Postoperatively mice received warm Ringer's lactate solution (0.5 mL, subcutaneous) and buprenorphine (0.1 mg/kg, subcutaneous).

Vein graft PVAT manipulation

In routine rodent vein graft surgery as well as in our first cohort of vein graft dietary intervention experiments, the donor caval vein was partially trimmed of its surrounding PVAT to facilitate end-to-end anastomosis creation in the recipient. In a follow-up cohort of C57BL/6J, we either completely stripped the donor caval vein of its surrounding PVAT or left all PVAT intact. The donor caval vein (with/without PVAT) was then transplanted into a recipient RCCA on a matched diet to the recipient (Control or MetR), to create a vein graft with PVAT intact, or a vein graft lacking PVAT. This resulted in four separate groups evaluating the interplay of diet and the presence of PVAT around the vein graft: Control − PVAT, Control + PVAT, MetR − PVAT, MetR + PVAT. Stripped donor venous PVAT was snap frozen in liquid nitrogen and then stored at −80 °C for subsequent analyses.

Vein graft/RCCA POD28 harvest

Under isoflurane anesthesia, mice were euthanized via exsanguination, followed by the insertion of a 21G needle in the left ventricle. Whole-body perfusion was performed with Ringer's lactate solution for 3 min, and followed by 3 min of perfusion-fixation with 10% formalin. The graft/RCCA was excised en-bloc via a midline neck incision and transferred to a 10% formalin (in PBS) solution for 24 h. After 24 h the tissue was transferred to a 70% ethanol solution for further processing as described below.

Baseline studies

To study effects of diet without surgery, baseline data were obtained from mice fed an identical dietary intervention (3-week Control diet followed by 1-week MetR or Control) and harvested after 1 week of MetR/Control. All tissue was collected on dry ice and snap frozen in liquid nitrogen, before storage at −80 °C. For baseline harvest, mice were first anesthetized, and a cardiac puncture was performed to collect 1 mL of whole blood in a 1.5 mL ethylenediaminetetraacetic acid (EDTA)-coated Eppendorf for downstream blood analysis. A thoracotomy was performed and caval vein PVAT was carefully dissected from the vessel wall with forceps. The caval vein was then harvested, after which caval vein wall and PVAT were stored separately. Lungs and heart were removed and thoracic aorta PVAT was carefully separated from the vessel wall, followed by harvest of the aortic wall. Both thoracic aorta and caval vein PVAT were stored separately.

Vein graft POD1 harvest

For vein graft POD1 harvest, after mice were anesthetized, the neck suture was removed and the surgical field from the previous day was opened. Vein graft patency was first ensured visually. In one cohort of mice, up to 1 mL whole blood was collected via cardiac puncture in an

https://doi.org/10.1038/s41467-024-53844-8

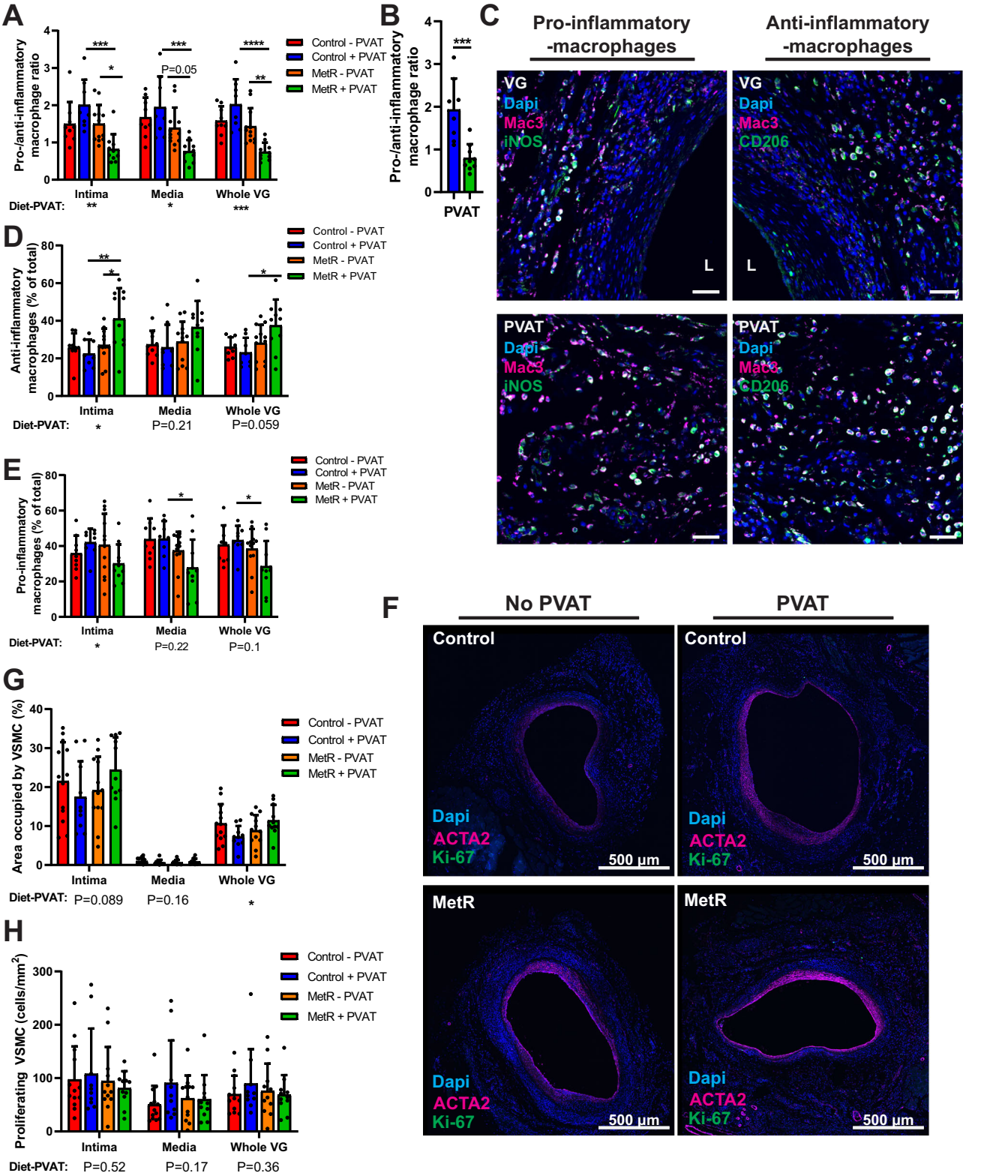

Fig. 5 | Favorable vein graft wall composition seen in MetR mice is also perivascular adipose tissue dependent. A Pro-/anti-inflammatory macrophage ratio per vein graft layer (intima; $^{*}p = 0.0278$, $^{***}p = 0.0003$) (media; $^{***}p = 0.0005$) (whole VG; $^{**}p = 0.0076$). **B** Pro-/anti-inflammatory macrophage ratio in PVAT of MetR and Control mice ($^{***}p = 0.0007$). **C** Immunohistochemical staining for pro- and anti-inflammatory macrophages, L indicates lumen. Scale bars = 500 µm. **D** Anti-inflammatory macrophages as a percentage of total MΦ per vein graft layer (intima; $^{*}p = 0.0206$, $^{**}p = 0.0043$) (whole VG; $^{*}p = 0.0183$). **E** Pro-inflammatory macrophages as a percentage of total MΦ per vein graft layer (media; $^{*}p = 0.0368$) (whole VG; $^{*}p = 0.0489$) (**A**, **B**, **D**, **E**; Control − PVAT $n = 9$, Control + PVAT $n = 8$, MetR − PVAT $n = 12$, MetR + PVAT $n = 10$). **F** Immunohistochemical staining for ACTA2 and Ki-67. Scale bars = 500 µm **G** Area occupied by VSMC per vein graft layer. **H** Proliferating VSMC (ACTA2 + Ki-67 double positive cells) per mm² per vein graft layer (**G**, **H**; Control − PVAT $n = 13$, Control + PVAT $n = 10$, MetR − PVAT $n = 12$, MetR + PVAT $n = 11$). All statistical testing was done via two-way ANOVA with Tukey's multiple comparisons test, unless otherwise indicated. $^{*}p < 0.05$, $^{**}p < 0.01$, $^{***}p < 0.001$, $^{****}p < 0.0001$. Source data are provided as a Source Data file.

Table 2 | Percentage of variation between groups that can be explained by diet, PVAT or a diet–PVAT interaction

Parameter	Source of variation	% of total variation	p value	p value summary	Parameter	Source of variation	% of total variation	p value	p value summary
Pro-/anti-inflammatory macrophage ratio Intima (Fig. 5A)	Interaction	20.38	0.0016	**	Pro-inflammatory macrophages Intima (Fig. 5E)	Interaction	10.33	0.0489	*
	PVAT +/−	0.3913	0.6384	ns		PVAT +/−	0.6856	0.6025	ns
	Diet	20.11	0.0017	**		Diet	1.899	0.3876	ns
Pro-/anti-inflammatory macrophage ratio Media (Fig. 5A)	Interaction	10.70	0.018	*	Pro-inflammatory macrophages Media (Fig. 5E)	Interaction	3.346	0.2238	ns
	PVAT +/−	1.663	0.3345	ns		PVAT +/−	2.986	0.2500	ns
	Diet	28.19	0.0003	***		Diet	17.65	0.0074	**
Pro-/anti-inflammatory macrophage ratio Whole VG (Fig. 5A)	Interaction	19.86	0.0006	***	Pro-inflammatory macrophages Whole VG (Fig. 5E)	Interaction	6.346	0.1039	ns
	PVAT +/−	0.9584	0.4160	ns		PVAT +/−	2.260	0.3259	ns
	Diet	31.89	<0.0001	****		Diet	11.99	0.0278	*
Anti-inflammatory macrophage Intima (Fig. 5D)	Interaction	12.01	0.0173	*	MΦ-macrophages Intima (Fig. S10C)	Interaction	20.02	0.0054	**
	PVAT +/−	4.668	0.1284	ns		PVAT +/−	0.1291	0.8133	ns
	Diet	15.95	0.0068	**		Diet	0.00009889	0.9948	ns
Anti-inflammatory macrophages Media (Fig. 5D)	Interaction	4.024	0.2121	ns	MΦ-macrophages Media (Fig. S10C)	Interaction	0.8676	0.5669	ns
	PVAT +/−	1.793	0.4019	ns		PVAT +/−	0.2800	0.7446	ns
	Diet	7.059	0.1012	ns		Diet	8.404	0.0806	ns
Anti-inflammatory macrophages Whole VG (Fig. 5D)	Interaction	8.175	0.0594	ns	MΦ-macrophages Whole VG (Fig. S10C)	Interaction	0.4932	0.6300	ns
	PVAT +/−	2.186	0.3205	ns		PVAT +/−	14.91	0.0113	*
	Diet	14.73	0.0130	*		Diet	9.798	0.0372	*

Two-way ANOVA with Tukey's multiple comparison test on pro-/anti-inflammatory macrophage ratio and anti-inflammatory macrophages (left), anti-inflammatory macrophages and MΦ macrophages (right) in Fig. 5 and Fig. S10.
*$p < 0.05$, **$p < 0.01$, ***$p < 0.001$, ****$p < 0.0001$.

Table 3 | Percentage of variation between groups that can be explained by diet, PVAT or a diet–PVAT interaction

Parameter	Source of variation	% of total variation	p value	p value summary	Parameter	Source of variation	% of total variation	p value	p value summary
% VSMC of intima (Fig. 5G)	Interaction	6.622	0.0897	ns	VSMC/mm^2 Intima (Fig. S10E)	Interaction	4.246	0.1832	ns
	PVAT +/−	0.1041	0.8286	ns		PVAT +/−	0.008998	0.9506	ns
	Diet	1.583	0.4005	ns		Diet	1.033	0.5080	ns
% VSMC of media (Fig. 5G)	Interaction	4.430	0.1693	ns	VSMC/mm^2 Media (Fig. S10E)	Interaction	6.810	0.0860	ns
	PVAT +/−	0.1700	0.7855	ns		PVAT +/−	1.037	0.4962	ns
	Diet	0.1062	0.8296	ns		Diet	1.278	0.4504	ns
% VSMC of whole VG (Fig. 5G)	Interaction	13.01	0.0153	*	VSMC/mm^2 Whole VG (Fig. S10E)	Interaction	10.20	0.0355	*
	PVAT +/−	0.2532	0.7262	ns		PVAT +/−	1.095	0.4802	ns
	Diet	2.068	0.3194	ns		Diet	0.4385	0.6545	ns
VSMC + Ki-67 intima (Fig. 5H)	Interaction	0.9706	0.5219	ns	% collagen of intima (Fig. S10F)	Interaction	2.705	0.2627	ns
	PVAT +/−	0.01213	0.9428	ns		PVAT +/−	1.738	0.3681	ns
	Diet	1.456	0.4334	ns		Diet	3.099	0.2311	ns
VSMC + Ki-67 media (Fig. 5H)	Interaction	4.180	0.1743	ns	% collagen of media (Fig. S10F)	Interaction	0.05245	0.8773	ns
	PVAT +/−	3.468	0.2151	ns		PVAT +/−	1.229	0.4562	ns
	Diet	0.8681	0.5323	ns		Diet	2.802	0.2625	ns
VSMC + Ki-67 whole VG (Fig. 5H)	Interaction	2.150	0.3458	ns	% collagen of whole VG (Fig. S10F)	Interaction	0.7912	0.5427	ns
	PVAT +/−	0.5066	0.6458	ns		PVAT +/−	2.748	0.2591	ns
	Diet	0.6122	0.6135	ns		Diet	3.815	0.1848	ns

Two-way ANOVA with Tukey's multiple comparison test on either % of vein graft layers occupied by VSMC, VSMC/mm^2, VSMC colocalizing with Ki-67 or % of vein graft layers occupied by collagen, as depicted in graphs in Fig. 5 and Fig. S10.
*$p < 0.05$.

EDTA-coated Eppendorf for downstream analysis, and then the vein graft was removed for histology as follows. A thoracotomy was performed, followed by whole-body perfusion via the left ventricle with ringer's lactate solution. A 21G syringe containing O.C.T. (Tissue-Tek, # 25608-930) was carefully inserted in the brachiocephalic trunk oriented toward the RCCA. Next, O.C.T. was slowly released into the brachiocephalic trunk until the vein graft started to dilate. After placing an 8/0 suture around the distal cuff, it was tightened followed by a second suture around the proximal cuff. The now dilated vein graft was removed en-bloc and placed in a mold filled with O.C.T., then placed on dry ice and stored at −80 °C. In a second cohort of mice, the PVAT surrounding the vein graft was carefully removed using forceps and collected in a 1.5 mL Eppendorf on dry ice. Next, the vein graft wall itself was taken out and collected in a separate Eppendorf on dry ice. Both PVAT and vein graft were then snap frozen in liquid nitrogen and stored at −80 °C.

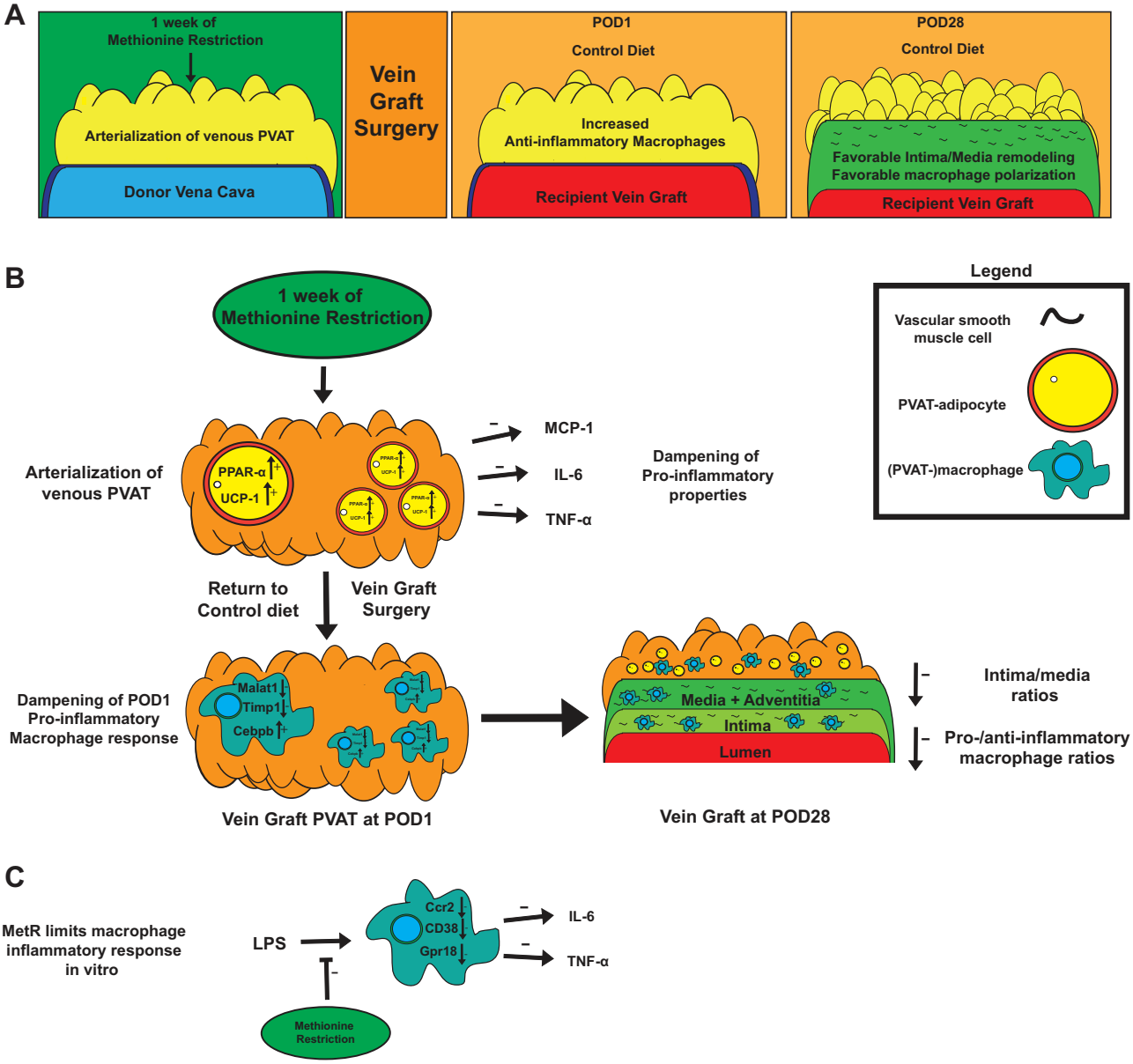

Fig. 6 | MetR modulates macrophage inflammation, induces PPAR-α induced browning in perivascular adipose tissue and protects from adverse vein graft remodeling. A General overview of proposed mechanism of MetR–PVAT interaction dependent protection from adverse vein graft remodeling. **B** In vivo/ex vivo mechanisms of MetR–PVAT interactions at preoperative, POD1 and POD28 timepoints. **C** Effects of MetR on macrophages in vitro.

Vein graft/RCCA histology

POD28 vein grafts and RCCA at POD28 after focal stenosis were harvested, embedded in paraffin, and cut in 5 μm sections by microtome, then mounted on slides. Sections were collected at regular intervals of 200 μm, starting from the proximal cuff until 1000 μm post proximal cuff. Focal stenosis arteries were cut at regular intervals of 400 μm, starting at 400 μm proximal from the focal stenosis, until 2800 μm proximal from the stenosis. For histomorphometric analysis, a Masson-Trichrome staining was performed: after deparaffinization to 95% ethanol, slides were immersed in 5% picric acid (in 95% ethanol) for 3 min, followed by a 3-min stain in working Harris Hematoxylin Solution (Fisher Scientific, cat# 245-678). After a brief tap water wash, slides were stained with 1% Biebrich scarlet in 1% acetic acid (Fisher Scientific, cat# A38S-500) for 3 min, followed by a quick rinse in distilled water. Slides were then stained for 1 min in 5% phosphomolybdic/phosphotungstic acid solution and immediately transferred to 2.5% light green SF yellowish in 2.5% acetic acid (Fisher Scientific, cat# A38S-500) for 4 min. Followed by a quick rinse in distilled water and a 2-min rinse in 1% acetic acid solution (Fisher Scientific, cat# A38S-500). After dehydration with xylene, slides were set with a cover glass using Permount mounting media (Electron Microscopy Science, cat# 17986-05). Brightfield images of vein graft and carotid artery cross sections were taken with a Zeiss Axio A1 microscope (Carl Zeiss). Histomorphometric analysis was performed using ImageJ 1.51p (Java 1.8.0_66) (see below).

Histomorphometric analysis

For vein graft histomorphometric analysis, images of cross sections taken at 200, 400, 600, 800, 1000 and 1200 μm post-cuff were uploaded in ImageJ. One cross section per distance was analyzed. Area and perimeter of lumen, internal elastic lamina and adventitial border were measured in $\mu m^2/\mu m$. The distinction between intima and media is based on the cellular orientation and alignment of elastin fiber in the vein graft wall. These analyses are performed by two, blinded, experienced observers. Next, lumen area, intimal area, intimal

thickness, media + adventitia (M) area, M thickness, intimal/media + adventitia (I/M) area ratio and I/M thickness ratio were calculated as described previously[72]. Two hundred micrometers to 1000 μm cross sections were next averaged into a per-vein graft histomorphometric endpoint. For focal stenosis histomorphometric analysis, RCCA cross-section images taken at 400, 800, 1200, 1600 and 2000 μm proximal from the focal stenosis were uploaded in ImageJ. Lumen area and perimeter, internal elastic lamina area and perimeter, external elastic lamina area and perimeter were measured. Next, lumen area, intimal area and thickness, medial area and thickness and I/M area and thickness ratios were calculated. Collagen measurements were performed via the color deconvolution function in ImageJ, the resulting split green area was measured via pixel threshold and normalized to total intimal/M and total vein graft area in %.

Immunohistochemistry

First, vein graft slides were incubated for 30 min at 60 °C in a vacuum oven, followed by immediate deparaffinization. Next, antigen retrieval was performed for 30 min at 97 °C in citrate buffer (pH 6.0) [Abcam, ab93678]. Then, slides were pre-incubated with 10% goat serum (Life Technologies, 50062Z) in PBS with 0.3 M glycine (Aijomoto, R015N0080039) for 1 h at room temperature (RT). Slides were then incubated with primary antibodies. For VSMC + KI-67 double staining: ACTA2 (mouse anti-mouse, Abcam, ab7817, 1:800) and Ki-67 (rabbit anti-mouse, Abcam, ab16667, 1:100). For M1/M2 macrophage staining, 1 vein graft slide containing 2–4 cross sections was double stained with the general macrophage marker Mac-3 (rat anti-mouse, Fisher Scientific, B550292, 1:600) and either iNOS (rabbit anti-mouse, Abcam, ab3523, 1:100) for M1, or CD206 (rabbit anti-mouse, Abcam, ab64693, 1:800) for M2. Slides with primary antibodies were incubated overnight at 4 °C. Slides were then washed in PBS + Tween (PBST) and incubated in secondary antibody for 2 h at RT. For ACTA2 + Ki-67 double staining, slides were incubated with Alexa Fluor 647 (goat anti-mouse, A-32728) and Alexa Flour 568 (goat anti-rabbit, A-11011) at 1:600. For M1/M2 staining, slides were incubated with Alexa Fluor 568 (goat anti-rabbit, A-11011) and Alexa Fluor 647 (goat anti-rat, A-21247) at 1:600. After secondary antibody incubation, slides were washed in PBST and mounted with DAPI (Vector, CB-1000) or stained with Hoechst staining solution and mounted with anti-fade media as indicated. For immunohistochemistry (UCP1/PPAR-α staining) slides were deparaffinized, endogenous peroxidase was blocked with 0.3% H_2O_2 in PBS for 15 min (only for UCP1), followed by antigen retrieval in Tris EDTA buffer (DAKO Blue) for 10 min at 95 °C (UCP1) or 98 °C (PPAR-α). Then, slides were pre-incubated with blocking solution (PBS + 5% albumin (PBSA) for UCP1, or 2.5% PBSA + 1% goat serum for PPAR-α), after which slides were incubated overnight in a humidity chamber with primary antibodies: UCP1 (rabbit anti-mouse, Abcam, ab155117, 1:400), PPAR-α (rabbit anti-mouse, Thermo Fisher Scientific, BS-3614R, 1:200). Slides were then washed in PBST, incubated for 25 min in 0.3% H_2O_2 in PBS and washed again in PBST (only for PPAR-α). Secondary antibody (Envision anti-rabbit) was applied and slides were incubated for 45 min at RT in a humidity chamber. After incubation, slides were washed with PBST, incubate in DAB solution (1 mL of substrate + 1 drop of chromogen) for 7 min, washed with diH_2O, immersed in hematoxylin stain for 10 s and rinsed with running tap water. Slides were then dehydrated and mounted with Pertex and coverslips.

Immunohistochemical analysis

For fluorescent IHC, 20× images were taken with a Laser Scanning Confocal Microscope (Zeiss LSM800) and automatically stitched. For non-fluorescent IHC, 10× brightfield images were taken with a Zeiss Axio A1 microscope (Carl Zeiss) and stitched with Adobe Photoshop. Lumen area, intimal area, media area and PVAT area were defined and measured in ImageJ, based on the corresponding Masson-trichrome histology picture. For VSMC + Ki-67 double staining analysis, 1 cross-section per vein graft was analyzed (600 or 800 μm). Based on Hoechst/DAPI staining, the lumen, intima and media area was measured in mm^2. The ACTA2 positive fluorescent (647 nm) channel was analyzed for total ACTA2 positive pixels via color threshold and then normalized to its respective vein graft layer (intima, media or total vein graft) in %. A cell positive for both ACTA2 and Ki-67 was regarded as a "proliferating VSMC". Total proliferating VSMCs per vein graft layer were then counted and normalized to cells/mm^2. Total ACTA2 positive cells were counted per vein graft layer and normalized to VSMC/mm^2 per vein graft layer. For analysis of macrophage polarization, one slide per vein graft (at 800 μm) containing 2–4 cross sections was stained with Mac-3 + iNOS or Mac-3 + CD206. Lumen area, intimal area, media area and PVAT area were measured in mm^2. All cells positive for Mac-3 were determined macrophages (M_Θ). Pro-inflammatory macrophage were cells positive for Mac-3 and iNOS. Anti-inflammatory macrophage were cells positive for Mac-3 and CD206. In each cross-section the total number of M_Θ and pro-/anti-inflammatory macrophages per vein graft layer was counted and normalized to mm^2. Per vein graft layer, pro- and anti-inflammatory macrophages (in count per mm^2) were normalized as a percentage of the total M_Θ-macrophages present in that layer (also in count/mm^2). The resulting percentages were then used to calculate a pro-/anti-inflammatory macrophage ratio.

For immunohistochemical analysis (UCP1/PPAR-α staining/adipocyte size) slides were automatically scanned using a 3DHISTECH slide scanner and images were uploaded in ImageJ. For the UCP1 and PPAR-α staining, the stain-positive PVAT-area was divided by the total PVAT area, which was manually selected. The positive area was quantified via intensity-based processing: the image was changed to HSB-brightness stack, in order to highlight the UCP1 positive area. Via thresholding, these areas were automatically selected, calculated and divided over the total PVAT area. To calculate the size of the adipocytes, Masson-Trichrome stained slides were used. First, the PVAT area was manually selected, after which customized scripts were used to automatically determine the adipocyte size. In brief, images were converted to grayscale and a threshold was set to create a black and white image. The image was then segmented using the watershed option in ImageJ to identify distinct adipocytes. The size was measured for all segmented adipocytes and plotted in a size-distribution graph.

Cell culture under MetR conditions

MetR medium was prepared by titrating 0% MetR medium (complete DMEM, Thermo Fisher Scientific, 21013-024, 10% FCS) with 100% MetR medium (complete DMEM without L-methionine and L-cysteine, Thermo Fisher Scientific, 11960-044, 10% FCS). For example, 1 part 0% MetR medium was mixed with three parts 100% MetR medium to create 75% MetR medium.

Bone marrow-derived macrophages

BMDM were harvested by removing the proximal and distal ends of both femur and tibia of multiple mice. Bones were flushed with cold PBS, collected through a cell strainer (70 μm) and spun down at 1000 rpm for 10 min. The pellet was washed with PBS and resuspended in 3 mL of ACK lysis buffer followed by 3 min of incubation on ice. Lysis was stopped by adding 7 mL of RPMI with 25% FCS, after which the suspension was washed twice with PBS. Cells were counted using a hemacytometer and seeded at 8×10^6 cells/dish (Falcon 100 × 15 mm) in 10 mL of medium (RPMI/25% FCS) with 20 μg/ml M-CSF. Medium was changed 7 days after seeding and after an additional 3 days cells were seeded at 300,000 cells/well in 24-well plates and left to adhere overnight. Cells were washed and Control or MetR medium supplemented with 10 ng/mL LPS (Sigma, K235) was added. After 24 h, medium was transferred to an Eppendorf and stored at −80 °C. Trizol was added to the cells and the plate was stored at −20 °C for RNA extraction.

3T3-L1 adipocytes

Murine 3T3-L1 preadipocytes (ATCC, CL-173) were differentiated into mature adipocytes by first incubating confluent cells in induction-medium (DMEM GlutaMAX™, Gibco®, 10% FCS) containing 1.6 µM insulin, 0.5 mM 1-methyl-3-isobutylxanthine (IBMX) and 0.25 µM dexamethasone. All medium contained 100 U/mL penicillin/streptomycin. After 2 days, cells were washed and differentiation-medium (DMEM GlutaMAX™, Gibco®, 10% FCS) containing 1.6 µM insulin was added and changed after 3 days. After an additional 3 days, cells were washed and maintained in regular culture medium (DMEM GlutaMAX™, Gibco®, 10% FCS) for 5 days, changing medium after 1 and 4 days. Differentiated 3T3-L1 adipocytes were washed and Control or MetR medium was added. After 48 h, medium was aspirated, TriPure RNA Isolation Reagent (Roche Diagnostics) was added to the adipocytes, and the plate was stored at −20 °C for RNA extraction.

Co-culture system

Murine 3T3-L1 preadipocytes were differentiated into mature adipocytes as described above. Similarly, BMDM were obtained as described above. Both cell types were cultured separately in both the transwell (VWR, #734-1579) as well as the bottom of 12-well plates. The cells that were cultured in the transwell were subjected to Control or 75% MetR medium, whilst the cells in the bottom were cultured in Control medium. Additionally, macrophages were stimulated with LPS to induce inflammation. After 24 h, medium was refreshed and cells were brought in co-culture by transferring the transwell to the corresponding "bottom" of a 12-well plates. Cells were co-cultured for 24 h on Control medium after which supernatant was collected (and stored at −80 °C) and Trizol was added to the cells (and stored at −20 °C). For schematic overview, see Fig. 4N, P.

Ex vivo PVAT studies

PVAT was carefully stripped in vivo from the caval vein and pooled in cold PBS. The tissue was washed by transporting into a fresh tube with PBS and thereafter weighed in separate Eppendorf tubes. After weighing, the tissue was transported into separate wells in a 24-well plates. Tissue was cultured under MetR or Control conditions for 24 h, medium was then transferred to an Eppendorf and stored at −80 °C. Trizol was added to the tissue and the tissue was stored at −20 °C for later use.

ELISA

Mouse TNF (BD Biosciences, cat. No. 558534), IL-6 (BD Biosciences, cat. No. 555240) and CCL2 (BD Biosciences, cat. No. 555260) ELISA's were used to quantify cytokine levels in PVAT and BMDM medium according to the manufacturer's protocol. Cytokine concentrations were corrected for the mass of PVAT of each sample.

RNA isolation from ex vivo and in vitro samples

VSMCs and BMDMs. 1 mL Trizol (Invitrogen 15596026) was added to each well and pipetted up and down once before transferring to 1.5 mL Eppendorf and incubating for 5 min at RT.

PVAT. Tissue samples were pooled in a 1.5 mL Eppendorf, that was cooled beforehand on dry ice, and 250 mL Trizol was added, after which the tissues were homogenized with a hand-held homogenizer (Fisherbrand) and 1.5 mL sterilized pestle (Axygen, PES 15-B-SI). After homogenization, the sample was centrifuged at 12,000 × *g* for 5 min at 4 °C. The supernatant was then transferred to a new Eppendorf tube followed by 5 min incubation at RT. Next, 200 µL of chloroform was added, the tubes vortexed and incubated for 2 min on wet ice. Tubes were then centrifuged at 12,000 × *g* for 10 min at 4 °C. The supernatant was collected and combined with 1 µL glycogen and 500 µL isopropanol, incubated for 10 min at RT and centrifuged at 12,000 × *g* for 10 min at 4 °C. The supernatant was discarded and 1 mL 75% ethanol was added followed by centrifugation at 13,000 × *g*, 15 min at 4 °C (twice). The final pellet was dried, resuspended in 20 µL RNAse-free water, quantified with NanoDrop 1.000 Spectrophotometer (Thermo Fisher Scientific) and stored at −80 °C. cDNA was synthesized using a High-Capacity cDNA Reverse Transcription Kit (Applied Biosystems) according to the manufacturer's protocol. qPCR was performed on a Quant Studio 5 qPCR machine (Applied Biosystems) using Taqman gene expression assays for *Hprt1*, *Tnfa*, *Ccl2*, *Il6*, *Leptin* and *Ppara* or Sybr Green for *Tnc*, *Lox*, *Ucp1*, *Ccr2*, *Cd38*, *Gpr18* and *Arg1* according to manufacturer's protocol.

Primer sequences	
mmu Ucp1 FW_1	TACCCAAGCGTACCAAGCTG
mmu Ucp1 RV_1	ACCCGAGTCGCAGAAAAGAA
mmu Ccr2 FW_1	AGTTCAGCTGCCTGCAAAGA
mmu Ccr2 RV_1	GCCGTGGATGAACTGAGGTA
mmu Cd38 FW_1	GAAGATGCCTGTGGTGTGGT
mmu Cd38 RV_1	TTCGATGTCGTGCATCACCC
mmu Gpr18 FW_1	ACACAGCACAGAGACACCAC
mmu Gpr18 RV_1	GCTGGCTCCCATGGTATGTA
mmu Arg1 FW_1	GGAAGAGTCAGTGTGGTGCT
mmu Arg1 RV_1	GGTTGTCAGGGGAGTGTTGA
mmu Tnc1 FW_1	TTTGCCCTCACTCCCGAAG
mmu Tnc1 rv_1	AGGGTCATGTTTAGCCCACTC
mmu Lox1 FW_1	CAGCCACATAGATCGCATGGT
mmu Lox1 RV_1	GCCGTATCCAGGTCGGTTC

RNA isolation from arterial and venous PVAT

PVAT samples were collected on dry ice, snap frozen in liquid nitrogen and stored at −80 °C. For RNA sequencing analysis of arterial (thoracic aorta) PVAT, the PVAT of two mice on matched diets was pooled in one pre-cooled Eppendorf tube on dry ice. For venous (caval vein) and vein graft PVAT RNA sequencing, PVAT from three mice on matched diets was pooled in one pre-cooled Eppendorf tube on dry ice. Next, 250 µL Trizol (Thermo Fisher Scientific, cat# 15596026) was added per sample and the tissue was thoroughly homogenized with a hand-held tissue homogenizer. After homogenization, samples were centrifuged at 12,000 × *g*, 5 min at 4 °C. Supernatant was transferred to a fresh tube and incubated for 5 min at RT, then 200 µL of chloroform (Sigma-Aldrich, cat#288306-1L) was added and the tube incubated for 2 min on wet ice. After centrifuging tubes at 12,000 × *g* for 10 min at 4 °C, the aqueous layer was collected in a fresh tube on ice. Two hundred fifty microliters of isopropanol and 1 µL glycogen were added to each sample, vortexed and centrifuged at 12,000 × *g*, 10 min at 4 °C. The supernatant was aspirated and 75% EtOH was added followed by vortexing and centrifugation at 12,000 × *g*, 10 min at 4 °C. The EtOH wash was repeated for a total of three times, then the RNA pellet was left to dry for 20 min at RT. The pellet was resuspended in 20 µL of RNAase-free H_2O and stored at −80 °C.

Bulk RNA sequencing

RNA concentration and purity was measured using a Nanodrop spectrophotometer and validated with an Agilent 2100 Bioanalyzer. cDNA libraries were prepared using the Illumina TruSeq Stranded Total RNA sample preparation protocol. cDNA libraries were pooled and sequenced on an Illumina NovaSeq 6000 at a depth of ~20 million paired-end 150 bp reads per sample. Reads were aligned to the mouse GRCm38.p6 assembly using the align function and annotated using the featureCounts function from the Rsubread R package

(version 2.3.7)[73]. Differential expression analysis was performed using the edgeR[74] (3.30.3) and limma[75] (3.44.3) R packages. ENSEMBL gene IDs were mapped to gene symbols and Entrez IDs using the mapIds function from the AnnotationDbi package (1.51.1). In total, reads were mapped to 27,179 genes. Read counts were normalized to counts per million reads (CPM) and genes that did not have at least one CPM in at least two samples were filtered, leaving 13,667 genes. Normalization was performed using the trimmed mean of M-values method as implemented in the calcNormFactors from edgeR. Data were modeled and differential expression was determined using the limma voom pipeline to generate linear models with empirical Bayes moderation. Differential expression was determined using a Benjamini–Hochberg adjusted p value < 0.05. Once differentially expressed genes were determined, gene set enrichment analysis was performed using the enrichKEGG function from the clusterProfiler package (3.16.0)[76].

Single nuclear sequencing

Nuclei from flash frozen tissues ($n = 2$/group) were isolated by mechanical dissociation with a glass homogenizer as previously described[77,78]. Homogenization was performed with a 7 mL glass Dounce tissue grinder (8–10 strokes with loose pestle, 8–10 strokes with tight pestle) in homogenization buffer (250 mM sucrose, 25 mM KCl, 5 mM $MgCl_2$, 10 mM Tris-HCl, 1 mM dithiothreitol (DTT), 1× protease inhibitor, 0.4 U μl^{-1} RnaseIn, 0.2 U μl^{-1} SUPERaseIn, 0.1% Triton X-100 in nuclease-free water). The nuclei suspension was filtered through a 40-µm cell strainer and centrifuged at 500 × g for 5 min for 4 °C. The supernatant was discarded and the pellet was resuspended in storage buffer (1× PBS, 4% bovine serum albumin (BSA), 0.2 U μl^{-1} Protector RnaseIn). Nuclei were stained with NucBlue Live ReadyProbes Reagents (Thermo Fisher Scientific) and Hoechst-positive single nuclei were purified by fluorescent activated cell sorting (FACS) using a FACSAria sorter (BD Biosciences). Nuclei purity and integrity were verified by microscope. cDNA libraries were prepared by loading nuclei suspension on a Chromium Controller (10X Genomics) with a targeted nuclei recovery number of 5000/sample followed by the Chromium Single Cell Reagent Kit v2 protocol (10X Genomics) according to the manufacturer's protocol. Quality control of individual and pooled cDNA libraries was performed with a Bioanalyzer 4200 TapeStation System (Agilent). Pooled libraries were sequenced using 150 bp paired-end reads on a NextSeq 500 (Illumina) at Harvard Medical School with a minimum depth of 20,000–30,000 read pairs per nucleus.

Following sequencing, Bcl files were converted to Fastq files using the Illumina bcl2fastq utility. Reads were mapped to the reference human transcriptome that was prebuilt with the 10X Genomics cellranger suite (v.3.0.1). Mapping quality was assessed using the cellranger summary statistics. Downstream analyses were performed using the Seurat R package (4.1.0)[79]. Briefly, cells were filtered for a minimum of 500 counts, minimum 200 genes and maximum 20% mitochondrial genes. Counts were log normalized and scaled at feature level. Clustering was performed using UMAP incorporating the first 15 components of PCA reduction. Clusters were determined using a shared nearest neighbor optimization with resolution of 0.2. Differential expression between clusters or between diets within clusters was performed using the FindMarkers function from the Seurat package. Gene set over-representation was performed using the enrichGO function from the ClusterProfiler package, using all GO ontologies with all observed genes within the cluster or clusters being analyzed serving as the background list.

Statistical analysis

All data are expressed as mean ± standard deviation unless indicated otherwise. Normality testing was performed employing the Shapiro–Wilk normality test. Normally distributed data were analyzed by Student's t-test, one-way or two-way ANOVA. Non-normally distributed data was analyzed by Mann–Whitney test. All statistical testing was two-sided and all testing was done via GraphPad Prism (8.4.2).

Reporting summary

Further information on research design is available in the Nature Portfolio Reporting Summary linked to this article.

Data availability

Data generated in this study are provided in the Source Data file. The nuclear RNA sequencing raw reads are deposited and freely accessible in the NIH Sequence Read Archive (SRA) under BioProject ID PRJNA1151602; PRJNA1151602 - SRA - NCBI (nih.gov). The bulk RNA sequencing raw reads are deposited and freely accessible in the NIH SRA under BioProject ID PRJNA1168893; ID 1168893 - BioProject - NCBI (nih.gov). Minimally processed RNA sequencing data are available on FigShare with the following DOIs: https://doi.org/10.6084/m9.figshare.26764840.v1, https://doi.org/10.6084/m9.figshare.26764837.v1. Source data are provided with this paper.

References

1. Farber, A. et al. Surgery or endovascular therapy for chronic limb-threatening ischemia. *N. Engl. J. Med.* **387**, 2305–2316 (2022).
2. Yahagi, K. et al. Pathophysiology of native coronary, vein graft, and in-stent atherosclerosis. *Nat. Rev. Cardiol.* **13**, 79–98 (2016).
3. de Vries, M. R. & Quax, P. H. A. Inflammation in vein graft disease. *Front. Cardiovasc. Med.* **5**, 3 (2018).
4. de Vries, M. R., Simons, K. H., Jukema, J. W., Braun, J. & Quax, P. H. A. Vein graft failure: from pathophysiology to clinical outcomes. *Nat. Rev. Cardiol.* **13**, 451–470 (2016).
5. Brown, N. K. et al. Perivascular adipose tissue in vascular function and disease: a review of current research and animal models. *Arterioscler. Thromb. Vasc. Biol.* **34**, 1621–1630 (2014).
6. Fernández-Alfonso, M. S. et al. Role of PVAT in coronary atherosclerosis and vein graft patency: friend or foe? *Br. J. Pharmacol.* **174**, 3561–3572 (2017).
7. Chatterjee, T. K. et al. Proinflammatory phenotype of perivascular adipocytes: influence of high-fat feeding. *Circ. Res.* **104**, 541–549 (2009).
8. Schroeter, M. et al. Leptin-dependent and leptin-independent paracrine effects of perivascular adipose tissue on neointima formation. *Arterioscler. Thromb. Vasc. Biol.* **33**, 980–987 (2013).
9. Manka, D. et al. Transplanted perivascular adipose tissue accelerates injury-induced neointimal hyperplasia: role of monocyte chemoattractant protein-1. *Arterioscler. Thromb. Vasc. Biol.* **34**, 1723–1730 (2014).
10. Nguyen, B. et al. Pre-operative diet impacts the adipose tissue response to surgical trauma. *Surgery* **153**, 584–593 (2013).
11. Longchamp, A. et al. Surgical injury induces local and distant adipose tissue browning. *Adipocyte* **5**, 163–174 (2016).
12. Mitchell, J. R. et al. Short-term dietary restriction and fasting precondition against ischemia reperfusion injury in mice. *Aging Cell* **9**, 40–53 (2010).
13. Mitchell, J. R., Beckman, J. A., Nguyen, L. L. & Ozaki, C. K. Reducing elective vascular surgery perioperative risk with brief preoperative dietary restriction. *Surgery* **153**, 594–598 (2013).
14. Longchamp, A., Harputlugil, E., Corpataux, J. M., Ozaki, C. K. & Mitchell, J. R. Is overnight fasting before surgery too much or not enough? How basic aging research can guide preoperative nutritional recommendations to improve surgical outcomes: a mini-review. *Gerontology* **63**, 228–237 (2017).
15. Robertson, L. T. et al. Protein and calorie restriction contribute additively to protection from renal ischemia reperfusion injury

partly via leptin reduction in male mice. *J. Nutr.* **145**, 1717–1727 (2015).
16. Hine, C. et al. Endogenous hydrogen sulfide production is essential for dietary restriction benefits. *Cell* **160**, 132–144 (2015).
17. Verweij, M. et al. Preoperative fasting protects mice against hepatic ischemia/reperfusion injury: mechanisms and effects on liver regeneration. *Liver Transplant.* **17**, 695–704 (2011).
18. Hine, C. & Mitchell, J. R. Calorie restriction and methionine restriction in control of endogenous hydrogen sulfide production by the transsulfuration pathway. *Exp. Gerontol.* **68**, 26–32 (2014).
19. Mauro, C. R. et al. Preoperative dietary restriction reduces intimal hyperplasia and protects from ischemia-reperfusion injury. *J. Vasc. Surg.* **63**, 500–509 (2014).
20. Trocha, K. M. et al. Short-term preoperative protein restriction attenuates vein graft disease via induction of cystathionine upsilon-lyase. *Cardiovasc. Res.* **116**, 416–428 (2019).
21. Kip, P. et al. Periprocedural hydrogen sulfide therapy improves vascular remodeling and attenuates vein graft disease. *J. Am. Heart Assoc.* **9**, e016391 (2020).
22. Orgeron, M. L. et al. The impact of dietary methionine restriction on biomarkers of metabolic health. *Prog. Mol. Biol. Transl. Sci.* **121**, 351–376 (2014).
23. Orentreich, N., Matias, J. R., DeFelice, A. & Zimmerman, J. A. Low methionine ingestion by rats extends life span. *J. Nutr.* **123**, 269–274 (1993).
24. Perrone, C. E. et al. Genomic and metabolic responses to methionine-restricted and methionine-restricted, cysteine-supplemented diets in Fischer 344 rat inguinal adipose tissue, liver and quadriceps muscle. *J. Nutrigenet. Nutrigenomics* **5**, 132–157 (2012).
25. Patil, Y. N., Dille, K. N., Burk, D. H., Cortez, C. C. & Gettys, T. W. Cellular and molecular remodeling of inguinal adipose tissue mitochondria by dietary methionine restriction. *J. Nutr. Biochem.* **26**, 1235–1247 (2015).
26. Hill, C. M. et al. FGF21 is required for protein restriction to extend lifespan and improve metabolic health in male mice. *Nat. Commun.* **13**, 1897 (2022).
27. Longchamp, A. et al. Amino acid restriction triggers angiogenesis via GCN2/ATF4 regulation of VEGF and H2S production. *Cell* **173**, 117–129.e114 (2018).
28. Trocha, K. et al. Preoperative protein or methionine restriction preserves wound healing and reduces hyperglycemia. *J. Surg. Res.* **235**, 216–222 (2019).
29. Plaisance, E. P. et al. Dietary methionine restriction increases fat oxidation in obese adults with metabolic syndrome. *J. Clin. Endocrinol. Metab.* **96**, E836–E840 (2011).
30. Wezel, A. et al. Deficiency of the TLR4 analogue RP105 aggravates vein graft disease by inducing a pro-inflammatory response. *Sci. Rep.* **6**, 24248 (2016).
31. Zhang, L., Hagen, P. O., Kisslo, J., Peppel, K. & Freedman, N. J. Neointimal hyperplasia rapidly reaches steady state in a novel murine vein graft model. *J. Vasc. Surg.* **36**, 824–832 (2002).
32. Goh, F. G., Piccinini, A. M., Krausgruber, T., Udalova, I. A. & Midwood, K. S. Transcriptional regulation of the endogenous danger signal tenascin-C: a novel autocrine loop in inflammation. *J. Immunol.* **184**, 2655–2662 (2010).
33. Rodríguez, C. et al. Regulation of lysyl oxidase in vascular cells: lysyl oxidase as a new player in cardiovascular diseases. *Cardiovasc. Res.* **79**, 7–13 (2008).
34. Arun, G., Aggarwal, D. & Spector, D. L. MALAT1 long non-coding RNA: functional implications. *Noncoding RNA* **6**, 22 (2020).
35. Ruffell, D. et al. A CREB-C/EBPβ cascade induces M2 macrophage-specific gene expression and promotes muscle injury repair. *Proc. Natl. Acad. Sci. USA* **106**, 17475–17480 (2009).
36. Bargut, T. C. L., Souza-Mello, V., Aguila, M. B. & Mandarim-de-Lacerda, C. A. Browning of white adipose tissue: lessons from experimental models. *Horm. Mol. Biol. Clin. Investig.* **31**, https://doi.org/10.1515/hmbci-2016-0051 (2017).
37. Orecchioni, M., Ghosheh, Y., Pramod, A. B. & Ley, K. Macrophage polarization: different gene signatures in M1(LPS+) vs. classically and M2(LPS–) vs. alternatively activated macrophages. *Front. Immunol.* **10**, 1084 (2019).
38. Li, W. et al. CD38: a significant regulator of macrophage function. *Front. Oncol.* **12**, 775649 (2022).
39. Jablonski, K. A. et al. Novel markers to delineate murine M1 and M2 Macrophages. *PLoS ONE* **10**, e0145342 (2015).
40. van Dam, A. D., Boon, M. R., Berbée, J. F. P., Rensen, P. C. N. & van Harmelen, V. Targeting white, brown and perivascular adipose tissue in atherosclerosis development. *Eur. J. Pharmacol.* **816**, 82–92 (2017).
41. Fitzgibbons, T. P. et al. Similarity of mouse perivascular and brown adipose tissues and their resistance to diet-induced inflammation. *Am. J. Physiol. Heart Circ. Physiol.* **301**, H1425–H1437 (2011).
42. Hasek, B. E. et al. Remodeling the integration of lipid metabolism between liver and adipose tissue by dietary methionine restriction in rats. *Diabetes* **62**, 3362–3372 (2013).
43. Wanders, D. et al. UCP1 is an essential mediator of the effects of methionine restriction on energy balance but not insulin sensitivity. *FASEB J.* **29**, 2603–2615 (2015).
44. Jonsson, W. O. et al. Physiologic responses to dietary sulfur amino acid restriction in mice are influenced by Atf4 status and biological sex. *J. Nutr.* **151**, 785–799 (2021).
45. Yu, D. et al. Short-term methionine deprivation improves metabolic health via sexually dimorphic, mTORC1-independent mechanisms. *FASEB J.* **32**, 3471–3482 (2018).
46. Stone, K. P. et al. Compromised responses to dietary methionine restriction in adipose tissue but not liver of ob/ob mice. *Obesity* **23**, 1836–1844 (2015).
47. Decano, J. L. et al. Systems approach to discovery of therapeutic targets for vein graft disease: PPARα pivotally regulates metabolism, activation, and heterogeneity of macrophages and lesion development. *Circulation* **143**, 2454–2470 (2021).
48. Gu, W. et al. Single-cell RNA-sequencing and metabolomics analyses reveal the contribution of perivascular adipose tissue stem cells to vascular remodeling. *Arterioscler. Thromb. Vasc. Biol.* **39**, 2049–2066 (2019).
49. Wanders, D. et al. FGF21 mediates the thermogenic and insulin-sensitizing effects of dietary methionine restriction but not its effects on hepatic lipid metabolism. *Diabetes* **66**, 858–867 (2017).
50. Fisher, F. M. et al. FGF21 regulates PGC-1α and browning of white adipose tissues in adaptive thermogenesis. *Genes Dev.* **26**, 271–281 (2012).
51. Wanders, D., Ghosh, S., Stone, K. P., Van, N. T. & Gettys, T. W. Transcriptional impact of dietary methionine restriction on systemic inflammation: relevance to biomarkers of metabolic disease during aging. *BioFactors* **40**, 13–26 (2014).
52. Jiang, Z. et al. Tumor necrosis factor-alpha and the early vein graft. *J. Vasc. Surg.* **45**, 169–176 (2007).
53. Owens, C. D. et al. Early remodeling of lower extremity vein grafts: inflammation influences biomechanical adaptation. *J. Vasc. Surg.* **47**, 1235–1242 (2008).
54. Tseng, C.-N. et al. Contribution of endothelial injury and inflammation in early phase to vein graft failure: the causal factors impact on the development of intimal hyperplasia in murine models. *PLoS ONE* **9**, e98904 (2014).

55. Dos Santos, L. M. et al. Methionine and methionine sulfoxide treatment induces M1/classical macrophage polarization and modulates oxidative stress and purinergic signaling parameters. *Mol. Cell. Biochem.* **424**, 69–78 (2017).
56. Zajac, E. et al. Angiogenic capacity of M1- and M2-polarized macrophages is determined by the levels of TIMP-1 complexed with their secreted proMMP-9. *Blood* **122**, 4054–4067 (2013).
57. Qiu, S. & Sun, J. lncRNA-MALAT1 expression in patients with coronary atherosclerosis and its predictive value for in-stent restenosis. *Exp. Ther. Med.* **20**, 129 (2020).
58. Zhao, G., Su, Z., Song, D., Mao, Y. & Mao, X. The long noncoding RNA MALAT1 regulates the lipopolysaccharide-induced inflammatory response through its interaction with NF-κB. *FEBS Lett.* **590**, 2884–2895 (2016).
59. Karper, J. C. et al. Toll-like receptor 4 is involved in human and mouse vein graft remodeling, and local gene silencing reduces vein graft disease in hypercholesterolemic APOE*3Leiden mice. *Arterioscler. Thromb. Vasc. Biol.* **31**, 1033–1040 (2011).
60. Souza, D. S., Christofferson, R. H., Bomfim, V. & Filbey, D. "No-touch" technique using saphenous vein harvested with its surrounding tissue for coronary artery bypass grafting maintains an intact endothelium. *Scand. Cardiovasc. J.* **33**, 323–329 (1999).
61. Dreifaldt, M. et al. The "no-touch" harvesting technique for vein grafts in coronary artery bypass surgery preserves an intact vasa vasorum. *J. Thorac. Cardiovasc. Surg.* **141**, 145–150 (2011).
62. Deb, S. et al. SUPERIOR SVG: no touch saphenous harvesting to improve patency following coronary bypass grafting (a multi-centre randomized control trial, NCT01047449). *J. Cardiothorac. Surg.* **14**, 85 (2019).
63. Tian, M. et al. No-touch versus conventional vein harvesting techniques at 12 months after coronary artery bypass grafting surgery: multicenter randomized, controlled trial. *Circulation* **144**, 1120–1129 (2021).
64. Greenstein, A. S. et al. Local inflammation and hypoxia abolish the protective anticontractile properties of perivascular fat in obese patients. *Circulation* **119**, 1661–1670 (2009).
65. Ketonen, J., Shi, J., Martonen, E. & Mervaala, E. Periadventitial adipose tissue promotes endothelial dysfunction via oxidative stress in diet-induced obese C57Bl/6 mice. *Circ. J.* **74**, 1479–1487 (2010).
66. Bays, H. E. Adiposopathy is "sick fat" a cardiovascular disease? *J. Am. Coll. Cardiol.* **57**, 2461–2473 (2011).
67. Zhu, X. et al. Perivascular adipose tissue dysfunction aggravates adventitial remodeling in obese mini pigs via NLRP3 inflammasome/IL-1 signaling pathway. *Acta Pharmacol. Sin.* **40**, 46–54 (2019).
68. Krom, Y. D. et al. Inhibition of neointima formation by local delivery of estrogen receptor alpha and beta specific agonists. *Cardiovasc. Res.* **73**, 217–226 (2007).
69. Plaisance, E. P. et al. Role of beta-adrenergic receptors in the hyperphagic and hypermetabolic responses to dietary methionine restriction. *Am. J. Physiol. Regul. Integr. Comp. Physiol.* **299**, R740–R750 (2010).
70. Hasek, B. E. et al. Dietary methionine restriction enhances metabolic flexibility and increases uncoupled respiration in both fed and fasted states. *Am. J. Physiol. Regul. Integr. Comp. Physiol.* **299**, R728–R739 (2010).
71. Tao, M. et al. A simplified murine intimal hyperplasia model founded on a focal carotid stenosis. *Am. J. Pathol.* **182**, 277–287 (2013).
72. Yu, P., Nguyen, B. T., Tao, M., Bai, Y. & Ozaki, C. K. Mouse vein graft hemodynamic manipulations to enhance experimental utility. *Am. J. Pathol.* **178**, 2910–2919 (2011).
73. Liao, Y., Smyth, G. K. & Shi, W. The R package Rsubread is easier, faster, cheaper and better for alignment and quantification of RNA sequencing reads. *Nucleic Acids Res.* **47**, e47 (2019).
74. Chen, Y., Lun, A. T. & Smyth, G. K. From reads to genes to pathways: differential expression analysis of RNA-Seq experiments using Rsubread and the edgeR quasi-likelihood pipeline. *F1000Research* **5**, 1438 (2016).
75. Ritchie, M. E. et al. limma powers differential expression analyses for RNA-sequencing and microarray studies. *Nucleic Acids Res.* **43**, e47 (2015).
76. Wu, T. et al. clusterProfiler 4.0: a universal enrichment tool for interpreting omics data. *Innovation* **2**, 100141 (2021).
77. Reichart, D. et al. Pathogenic variants damage cell composition and single cell transcription in cardiomyopathies. *Science* **377**, eabo1984 (2022).
78. Litviňuková, M. et al. Cells of the adult human heart. *Nature* **588**, 466–472 (2020).
79. Stuart, T. et al. Comprehensive integration of single-cell data. *Cell* **177**, 1888–1902.e1821 (2019).

Acknowledgements

This work was supported by an American Heart Association Post-Doctoral Grant [#19POST34400059] and grants from Foundation "De Drie Lichten", Prins Bernhard Cultural Foundation and Michael-van Vloten Foundation to P.K.; Rembrandt Institute for Cardiovascular Science to M.R.d.V.; American Heart Association Grant-in-Aid 16GRNT27090006; the National Institutes of Health (NIH), 1R01HL133500 to C.K.O.; the NIH (AG036712, DK090629) and Charoen Pokphand Group to J.R.M.; and the NIH (R01HL126901 and R01HL149302) to M.A.

Author contributions

P.K. provided funding, conceived of experimental designs, performed experiments and wrote the manuscript. T.S. conceived of experimental designs, performed in vitro/in vivo experiments and data analysis. M.T. performed surgeries, processed vein grafts and analyzed histology. P.H.Q. advised on analysis of vein grafts. J.W.J. assisted with ex vivo and in vitro experiments. J.G. and J.S. performed and advised on single-cell nuclear sequencing experiments. M.R.M. and S.J.M. assisted with animal care and in vivo studies, M.R.M. performed data analysis in bulk and nuclear RNA sequencing. S.K. advised on analysis of in vitro experiments, N.K. performed in vitro experiments. J.L.D. and M.A. advised on data interpretation. M.R.V., J.R.M. and C.K.O. provided funding, conceived of experimental designs and supervised the project. All authors reviewed and approved the final version of the submitted manuscript.

Competing interests

The authors declare no competing interests.

Additional information

Supplementary information The online version contains supplementary material available at https://doi.org/10.1038/s41467-024-53844-8.

Correspondence and requests for materials should be addressed to Margreet R. de Vries.

Peer review information *Nature Communications* thanks Qingbo Xu and the other, anonymous, reviewer(s) for their contribution to the peer review of this work. A peer review file is available.